Neurobiology of Disease

Demyelination Causes Adult CNS Progenitors to Revert to an Immature State and Express Immune Cues That Support Their Migration

Sarah Moyon,[1,2,3] Anne Laure Dubessy,[1,2,3] Marie Stephane Aigrot,[1,2,3] Matthew Trotter,[7] Jeffrey K. Huang,[6] Luce Dauphinot,[1,2,3] Marie Claude Potier,[1,2,3] Christophe Kerninon,[4] Stephane Melik Parsadaniantz,[8] Robin J. M. Franklin,[6] and Catherine Lubetzki[1,2,3,5]

[1]Université Pierre et Marie Curie-Paris 6, Centre de Recherche de l'Institut du Cerveau et de la Moelle Épinière, 75013 Paris, France, [2]Institut National de la Santé et de la Recherche Médicale, U 1127, 75013 Paris, France, [3]CNRS, Unite Mixte de Recherche 7225, 75013 Paris, France, [4]Institut Hospitalo Universitaire-A-Institut du Cerveau et de la Moelle Épinière, 75013 Paris, France, [5]Groupe Hospitalier Pitié-Salpêtrière, 75013 Paris, France, [6]Department of Clinical Neuroscience, Wellcome Trust-Medical Research Council Cambridge Stem Cell Institute, University of Cambridge, Cambridge CB3 0ES, United Kingdom, [7]Anne McLaren Laboratory for Regenerative Medicine, University of Cambridge, Forvie Site, Cambridge CB2 0SZ, United Kingdom, and [8]Institut de la Vision, UMRS 968, UMR 7210 CNRS, Université Pierre et Marie Curie-Paris 6, 75012 Paris, France

The declining efficiency of myelin regeneration in individuals with multiple sclerosis has stimulated a search for ways by which it might be therapeutically enhanced. Here we have used gene expression profiling on purified murine oligodendrocyte progenitor cells (OPCs), the remyelinating cells of the adult CNS, to obtain a comprehensive picture of how they become activated after demyelination and how this enables them to contribute to remyelination. We find that adult OPCs have a transcriptome more similar to that of oligodendrocytes than to neonatal OPCs, but revert to a neonatal-like transcriptome when activated. Part of the activation response involves increased expression of two genes of the innate immune system, *IL1β* and *CCL2*, which enhance the mobilization of OPCs. Our results add a new dimension to the role of the innate immune system in CNS regeneration, revealing how OPCs themselves contribute to the postinjury inflammatory milieu by producing cytokines that directly enhance their repopulation of areas of demyelination and hence their ability to contribute to remyelination.

Key words: **cytokines; migration; multiple sclerosis; Oligodendrocyte progenitor cells; remyelination**

Introduction

The adult CNS contains a widespread population of multipotent progenitor cells, commonly referred to as oligodendrocyte progenitor cells (OPCs; ffrench-Constant and Raff, 1986; Levine et al., 2001). While the physiological function of these cells in the normal CNS remains uncertain, it is well established that adult OPCs (aOPCs) are primarily responsible for generating new oligodendrocytes (OLs) and the restoration of myelin sheaths following demyelinating injury (Zawadzka et al., 2010). This regenerative process of remyelination can be highly efficient, especially after single episodes of demyelination in young adults (Shields et al., 1999). However, in chronic demyelinating disease, such as multiple sclerosis (MS), remyelination becomes less efficient, with the result that axons are left denuded and vulnerable to irreversible degeneration, leading to the accumulation of disability (Ferguson et al., 1997; Nave and Trapp, 2008). To develop therapies by which remyelination can be enhanced, it will be necessary to identify the key mechanisms that regulate remyelination.

At least three distinct phases of remyelination are identifiable, as follows: first, a process of activation, in which aOPCs in the vicinity of the injury change their shape and gene expression profile; second, aOPC recruitment into and within the demyelinated area by migration and proliferation; and third, differentiation of the recruited aOPCs into mature myelin sheath-forming oligodendrocytes (Levine and Reynolds, 1999). Ultimately, the successful orchestration of remyelination involves a complex in-

Received March 3, 2014; revised June 27, 2014; accepted July 21, 2014.

Author contributions: C.L. designed research; S.M., A.L.D., M.S.A., and C.K. performed research; J.K.H. and S.M.P. contributed unpublished reagents/analytic tools; S.M., M.T., L.D., M.C.P., and R.J.M.F. analyzed data; S.M., R.J.M.F., and C.L. wrote the paper.

This work was supported by grants from the Fondation ARSEP (R.J.M.F. and C.L.), the UK Multiple Sclerosis Society (R.J.M.F.), the French National Agency for Research, and the French Medical Research Foundation (A.L.D.). The research leading to these results has received funding from the program "Investissements d'avenir" ANR-10-IAIHU-06. We thank C. Blanc and B. Hoareau (Flow Cytometry Core CyPS, Pierre & Marie Curie University, Pitié-Salpêtrière Hospital, Paris, France) for their assistance on FACS; and D. Langui (Cellular Imaging Core, Pitié-Salpêtrière Hospital) for his assistance for videomicroscopy experiments; and P. Ravassard (Vectoroly Core Facility, Pitié-Salpêtrière Hospital). We also thank Dr. B. Nait-Oumesmar (Centre de Recherche de l'Institut du Cerveau et de la Moelle Épinière, UMRS 975, Paris) for analysis of multiple sclerosis lesions and the UK Multiple Sclerosis Society Brain Bank (Professor R. Reynolds, Imperial College, London, United Kingdom) for multiple sclerosis tissue. In addition, we thank Dr. P. Soriano for the *PDGFαR:GFP* transgenic line.

The authors declare that there are no conflicts of interest.

Correspondence should be addressed to either of the following: Catherine Lubetzki, Université Pierre et Marie Curie-Paris 6, Centre de Recherche de l'Institut du Cerveau et de la Moelle Épinière, 75013 Paris, France, E-mail: catherine.lubetzki@psl.aphp.fr; or Robin J. M. Franklin, Department of Clinical Neuroscience, Wellcome Trust-Medical Research Council Cambridge Stem Cell Institute, University of Cambridge, Cambridge CB3 0ES, United Kingdom, E-mail: rjf1000@cam.ac.uk.

DOI:10.1523/JNEUROSCI.0849-14.2015

 0270-6474/15/350004-17$15.00/0

terplay between environmental and cell intrinsic mechanisms in which the transition between each phase is appropriately timed (Franklin, 2002).

Genomic screening has already led to the identification of several important regulatory pathways and mechanisms by which remyelination is governed. These include the Wnt pathway, a negative regulator of differentiation and two positive regulatory mechanisms involving the nuclear receptor RXRγ (retinoid X receptor γ) and the transcription factor MRF (myelin gene regulatory factor; Emery et al., 2009; Fancy et al., 2009, 2011; Huang et al., 2011; Koenning et al., 2012). These studies testify to the value of gene-profiling approaches and prompted us to establish the gene profile of aOPCs in the normal physiological state and how it changes in response to demyelinating injury as aOPCs prepare to engage in remyelination.

Materials and Methods

Animals and cuprizone treatment. Neonatal OPCs (nOPCs) and aOPCs were isolated from the brain of either sex postnatal day 1 (P1) to P5 and 2-month-old *PDGFαR:GFP* hemizygous mice, respectively (Klinghoffer et al., 2002; RRID:IMSR_JAX:007669). Adult OPCs in demyelinating conditions (activated aOPCs) were isolated from the brain of either sex 2-month-old *PDGFαR:GFP* mice, previously treated for 5 weeks with cuprizone (0.2%; Sigma). Adult OLs were isolated from the brains of 2-month-old *PLP:GFP* homozygous mice of either sex (Spassky et al., 2001). Animal care and experiments were performed according to European Community regulations and ethics policies.

Fluorescent-activated cell sorting purification of GFP-positive oligodendrocytes and oligodendrocyte precursor cells. Isolation was performed in two steps, as described previously (Piaton et al., 2011). Briefly, brains from either *PDGFαR::GFP* mice (Klinghoffer et al., 2002; RRID:IMSR_JAX:007669) or *PLP-GFP* mice (Spassky et al., 2002) were used to obtain OPCs and oligodendrocytes, respectively. Tissue was dissected in HBSS 1× [HBSS 10× (Invitrogen), 0.01 M HEPES buffer, 0.75% sodium bicarbonate (Invitrogen), and 1% penicillin/streptomycin] and mechanically dissociated. After an enzymatic dissociation step using papain (30 μg/ml in DMEM-Glutamax, with 0.24 μg/ml L-cystein and 40 μg/ml DNase I), cells were put on a preformed Percoll density gradient before centrifugation for 15 min. Cells were then collected and stained with propidium iodide (PI) for 2 min at room temperature (RT). In a second step, GFP-positive and PI-negative cells were sorted by fluorescence-activated cell sorting (FACS; Aria, Becton Dickinson) and collected in pure fetal bovine serum. To ensure the sorting of a homogenous population of OPCs from adult *PDGFαR::GFP* brains, only the high GFP cells (selected using a cutoff of fluorescence intensity representing ~90% of the GFP cells) were sorted, as described by Piaton et al. (2011). For microarray analysis, cells were washed twice in PBS 1× (PBS 10×, Invitrogen), then the dry cell pellets were frozen at −80°C. For cultures, cells were maintained in modified Bottenstein–Sato (BS) medium (DMEM containing 0.5% FCS, 2 mM L-glutamine, 10 μM insulin, 5 ng/ml sodium selenite, 100 μg/ml transferrin, 0.28 μg/ml albumin, 60 ng/ml progesterone, 16 μg/ml putrescine, 40 ng/ml triiodothyronine, and 30 ng/ml L-thyroxine), before being platted on poly-L-lysine-coated glass coverslips (40 μg/ml, Sigma; for immunostaining and ELISA), on Matrigel-coated wells (1:10; BD Biosciences; for video microscopy), or on transwell xCELLingence inserts (Roche; for migration assay). To assess the differentiation, proliferation, and apoptosis of *in vitro* OPCs, recombinant proteins Il1β (5 ng/ml; R&D Systems) or Ccl2 (20 ng/ml; PeproTech) were added in BS medium. To assess differences in differentiation, we used a morphological classification of oligodendroglial development adapted from Huang et al. (2011), in which five stages were defined. For flow cytometry analysis, cells were fixed with 4% PFA, directly after the Percoll gradient. Then they were incubated with anti-O4-PE antibody [mouse IgM, dilution 1:11 for 10^6 cells/100 μl; catalog #130-095-887 (RRID:AB_10831029), Miltenyi Biotec] or control isotype [mouse IgM PE, dilution 1:11 for 10^6 cells/100 μl; catalog #130-093-177 (RRID:AB_871723), Miltenyi Biotec], for 30 min at RT in PBS 1×. Cells were analyzed using a LSR Fortessa flow cytometer (Becton Dickinson) and Diva software.

RNA extraction and microarray analysis. For each condition, we used four independently FACS samples, to provide four biological replicates. Total RNA was extracted using NucleoSpin RNA XS kit (Macherey-Nagel). Quantity and quality of RNA extractions were analyzed using Agilent RNA 6000 Pico kit (Agilent). Labeled RNAs (Liqa Kit, Agilent) were then hybridized onto Agilent whole-mouse genome microarray chips. Data were normalized and analyzed using the R statistical open tool (R Manuals; RRID:OMICS_01764). We used a Student's *t* test and Benjamini–Hochberg test to identify the differentially expressed genes between two conditions (cutoffs: $p < 0.001$ and $q < 0.01$, respectively). Gene expression levels and unsupervised hierarchical clustering were visualized using MultiExperiment Viewer version 4.6.0 open software (TM4 Microarray Software Suite: TIGR MultiExperiment Viewer; RRID:nif-0000-10486). The gene ontology enrichment analyses were performed using GOrilla open software. Ariadne Genomics-Pathway Studio software was used to select genes of interest. A full list of genes was deposited in NCBI GEO (Gene Expression Omnibus; RRID:nif-0000-00142; accession number: GSE48872).

Immunostaining. For immunohistochemistry, animals were perfused with 4% PFA in PBS 1×. The brains were dissected, and cryoprotected in PBS 1× and sucrose 15% at 4°C overnight, frozen embedded in gelatin 7% (gelatin porcine skin, Merck), sucrose 15%, PBS 1×; and 14 μm serial coronal cryostat sections were saved. Other brain samples were dissected, and maintained in PBS 1× in 20 μm serial coronal vibratome sections. The slides were treated for 10 min with 100% ethanol at −20°C, and, after saturation in PBS 1×, 0.3% Triton X-100, and 10% horse serum for 1 h at RT, primary antibodies were incubated overnight at 4°C in PBS 1×, 0.3% Triton X-100, and 5% horse serum. After washing, Alexa Fluor-conjugated and biotinylated secondary antibodies were incubated for 1.5 h at RT. Nuclei were stained with Hoechst solution (1 μg/ml), and sections were mounted in Fluoromount-G (CliniSciences). For immunocytochemistry, cells were fixed with 4% PFA for 15 min at RT, and staining was performed as described above, without the ethanol step. Staining was observed using a fluorescence microscope Zeiss Imager. Pictures were acquired with an AxioCam camera and analyzed using ImageJ software (ImageJ; RRID:nif-0000-30467). For quantification of Ccl2 and Il1β expression on coronal sections of demyelinated brains, only demyelinating areas, selected by the absence of or low myelin basic protein (MBP) staining, were quantified. Similar areas were quantified on control sections.

Antibodies. For immunostaining, antibodies were used at the following dilutions: anti-MBP [chicken IgY, 1:200; catalog #AB9348 (RRID:AB_2140366), Chemicon International/Millipore/Linco Research], anti-platelet-derived growth factor α receptor [PDGFαR; rat IgG2a, 1:800; catalog #562171 (RRID:AB_2307390), BD PharMingen], anti-GFP (rabbit polyclonal, 1:500; catalog #A6455 (RRID:AB_221570), Invitrogen], anti-cleaved caspase-3 [rabbit polyclonal, 1:500; catalog #AF835 (RRID:AB_2243952), R&D systems], anti-Ki-67 [mouse IgG1, 1:400; catalog #550609 (RRID:AB_2307388), BD-PharMingen], anti-Ccl2 (rabbit IgG, 1:1000, Torrey Pines Biolabs), anti-Ccl2 [mouse IgG1, clone 5D3-F7, 1:100; catalog #16-7099-85 (RRID:AB_469223), eBioscience; for human tissue], anti-Il1β [rabbit polyclonal, 1:100; catalog #ab9722, (RRID:AB_308765), Abcam], anti-Olig1 [mouse IgG2b, 1:400; catalog #MAB2417 (RRID:AB_2157534), R&D Systems], anti-Olig2 [rabbit polyclonal, 1:200; catalog #AB9610 (RRID:AB_570666), Chemicon International/Millipore/Linco Research], anti-Ccr2 [rabbit polyclonal, 1:200; catalog #ab21667 (RRID:AB_446468), Abcam], anti-A2B5 [mouse IgM, 1:5; catalog #MAB1416 (RRID:AB_357687), R&D Systems], anti O4 (mouse monoclonal IgM, 1:5; hybridoma was a gift from I. Sommer, University of Glasgow, UK), and anti-NG2 (rabbit polyclonal, 1:200; Millipore).

Quantitative PCRs. PCR primers for mouse *Il1β*, *Ccl2*, *Ccr2*, *Il1r1*, and *Ppia* were purchased from Qiagen. RT was performed using Verso cDNA Synthesis kit (Thermo Scientific). Real-time quantitative PCR (qPCR) was performed on the LightCycler 480 using the QuantiFast Probe Duplex Assays (Qiagen). Results were normalized against Ppia and expressed as the mean ± SEM.

Cell migration. Cell migration was assessed using the xCELLingence System (Roche). On top of the upper chamber, 25,000 FAC-sorted cells were plated. Control medium or medium containing the recombinant proteins Il1β (5 ng/ml; R&D systems) or Ccl2 (20 ng/ml; PeproTech), and/or their respective antagonists Il1ra1 (200 ng/ml; R&D systems) and INCB3344 (INCB, 8 μM; Chemscene) were distributed in the lower chambers. Cell migration was followed for 48 h. Each condition was run simultaneously in triplicate or quadriplicate. Results were expressed compared with control medium or with the migration of aOPCs under control conditions for each independent experiment ($n = 5$).

Video microscopy. FAC-sorted cells were plated on Matrigel-coated wells for 24 h. Cells were then monitored for 24 h (one picture every 10 min) using a Zeiss Axiovert 200 microscope and a Hamamatsu camera, in BS medium only (for control conditions and for transduced cells) or in BS medium with Il1β (5 ng/ml; R&D systems) or Ccl2 (20 ng/ml; PeproTech) recombinant proteins. MetaMorph tracking software was used to follow every cell (identified by a single colored spot), and quantify their motility and velocity. Three distinct positions and an average of 150 cells per well were analyzed.

ELISA. FAC-sorted cells were plated in 96-well plaques (100,000 cells per well, in 100 μl of BS). After 24 h, supernatants from FACs-purified aOPCs were collected, and cells were detached using trypsin (0.025%). Cells were then lysed in Tris (50 mM), pH 7.4, NaCl (150 mM), Triton 1%, and protease inhibitor cocktail (1:100; Sigma). The protein concentration in cell lysates was quantified using a BCA protein assay to normalize Ccl2 and Il1β expression. Ccl2 and Il1β expressions in cell supernatants and cell lysates were quantified following Mouse MCP-1 ELISAs and Mouse Il1β ELISAs, respectively (BioVendor).

CG4 culture. Rat CG4 cells were grown on poly-D-ornithine-coated (100 μg/ml) plastic Petri dishes in a mixture of N1 medium supplemented with B104 medium (30%) and biotin (10 ng/ml).

Lentiviral vector production. The plasmid insert pDONR221mm_ccl2 (a gift from Dr. S. Melik-Parsadaniantz, Institut de la Vision, Paris, France) has been completely sequenced before use. Lentiviral vectors were prepared through LR clonase II Gateway recombination (Invitrogen) to generate CMV_CCL2-2A-mCherry and CMV_DsRed-Myc. Lentiviral vector stocks were produced by transient transfection of human embryonic kidney (HEK) 293T cells with the p8.9 encapsidation plasmid, the VSV glycoprotein-G-encoding pHCMV-G plasmid, and the lentiviral recombinant vector. Supernatants were ultracentrifugated, and the pellets were resuspended in PBS 1×. Aliquots were kept at −80°C until use. The transduction efficiency of each lentivirus was evaluated using ELISA p24 titration kit (ZeptoMetrix) on HEK 293T cells.

Cell transduction and grafting. Two-month-old *PDGFαR:GFP* brain cells were isolated by Percoll gradient as previously described. Cells were resuspended in BS medium and plated on 25 cm^2 flasks. CG4 cells were maintained in N1 culture medium. Cells were then transduced for 24 h with either CMV_CCL2-2A-mCherry or CMV_DsRed-Myclentiviral vectors at a multiplicity of infection of 100, using DEAE-Dextran hydrochloride for OPCs, not for CG4 (1×; Sigma). Three days after the transduction, mCherry-positive or DsRed-positive cells (OPCs or CG4 cells) were FAC-sorted and plated back, or 100,000 CG4 cells were directly grafted in the anterior brain of postnatal 2-d-old *PDGFαR:GFP* mice. P2 *PDGFαR::GFP* mice were killed 40 h after the CG4 graft, and brains were dissected and frozen before being coronally cut by cryostat. For each brain, we accessed the maximal lateral, dorsoventral, and anteroposterior migration. We quantified the number of CG4 cells remaining at the injection site, which migrated over 300, 500, 800, and 1000 μm, and therefore calculated the percentage of moving cells. For each experiment, we analyzed three to six animals per condition.

Multiple sclerosis tissue samples. Fixed postmortem multiple sclerosis brain samples were obtained from the UK Multiple Sclerosis tissue Bank. Histological assessment of the lesions was performed using Luxol fast blue/cresyl violet and Oil-red-O (macrophages filled with myelin debris) histological staining. Lesions were classified according to their inflammatory activity (KP1 immunolabeling) and on the basis of histological criteria of acute lesions (active demyelination, myelin vacuolation, inflammation or edema, minor gliosis, and vague margin) and chronic lesions (no myelin vacuolation, absence of inflammation, gliosis, axonal loss, and sharp margin). The expression of Ccl2 was analyzed in active lesions ($n = 5$), the active border of chronic lesions ($n = 3$), the chronic silent core ($n = 4$), and normal-appearing white matter (NAWM, $n = 6$) from six different patients. For each lesion, we calculated the ratio of Ccl2 expression by aOPCs in the lesion normalized to the percentage in adjacent NAWM of the same size. Immunohistochemistry was performed as described above, with the addition of an initial pretreatment with an unmasking solution (low pH, citric acid; Vector Laboratories).

Statistical analyses. All quantifications were performed blindly. Statistical analysis was performed using GraphPad Prism version 6.0 software. Error bars on all graphs represent the SE.

Results

The gene expression profile of aOPCs in normal CNS resembles that of OLs

OLs are distinctive from the progenitor cells that give rise to them, and so, as expected, the two cells have distinctive gene expression profiles (Cahoy et al., 2008). However, the transcriptional profile of aOPCs in the normal intact CNS is unknown. Furthermore, since increased expression of genes associated with developmental myelination has been detected in aOPCs in response to demyelination in the adult CNS (Fancy et al., 2004; Shen et al., 2008), we first hypothesized that the transcriptome of the aOPCs would be distinct from that of the nOPCs, and, second, that the transcriptome of the aOPCs would revert to that of the nOPCs upon activation. To address the first of these, we compared gene profiles of aOPCs with those of nOPCs and OLs.

Adult OPCs were isolated by FACS from brains of 2-month-old *PDGFαR:GFP* transgenic mice (Klinghoffer et al., 2002; Hamilton et al., 2003) using a cutoff of fluorescence intensity to select high-GFP cells, as previously described (Piaton et al., 2011). To ensure that the GFP population, widely distributed in the adult CNS (Fig. 1*a*), consisted of aOPCs, we assessed their expression of NG2, a marker of OPCs, *in vivo*. Whereas 91.7 ± 1.7% of the GFP-positive cells expressed $NG2^+$, virtually all highly GFP-positive cells were NG2 positive (Fig. 1*b*). In contrast, low-expressing GFP cells (not exceeding 10% of the GFP-positive cells *in vivo*) were NG2 negative, possibly corresponding to differentiating cells.

Neonatal OPCs were isolated by FACS from the brains of P1–P5 *PDGFαR:GFP* transgenic mice. OLs were isolated by FACS from the brains of adult (2-month-old) *PLP-GFP* mouse in which GFP is restricted to mature OLs (Fig. 1*g*; Spassky et al., 2001; Le Bras et al., 2005).

Flow cytometry analysis showed that O4 was expressed by 72.8 ± 4.9% of cells sorted from *PDGFαR:GFP* neonatal brain, whereas it was expressed by 94.9 ± 1.6% of cells isolated from *PDGFαR:GFP* adult brain and 97.2 ± 2.3% of cells isolated from proteolipid protein *(PLP)-GFP* adult brains (Fig. 1*e–g*,*i–k*).

To further characterize sorted cells from *PDGFαR:GFP* adult brains, immunolabeling was performed, 1 h and 2 d after sorting, on cells cultured in modified BS medium. At both time points, GFP-sorted cells expressed markers of immature stages of the oligodendroglial lineage, such as O4 and NG2 (96% and 98%, respectively, quantification in one representative experiment), but also the marker of mature stages MBP [87%, quantification in one representative experiment; Fig. 2*a–c* (see triple labeling in *c*)]. This *in vitro* analysis supported the conclusion that the GFP-positive population isolated from adult *PDGFαR:GFP* transgenic mice were adult OPCs. In contrast, whereas OLs sorted from *PLP-GFP* adult brains expressed O4 and MBP, they did not express NG2 or PDGFαR (Fig. 2*d*).

Having characterized *in vitro* populations of nOPCs, aOPCs, and OLs, a microarray analysis of each cell population was undertaken with four independently sorted samples providing four

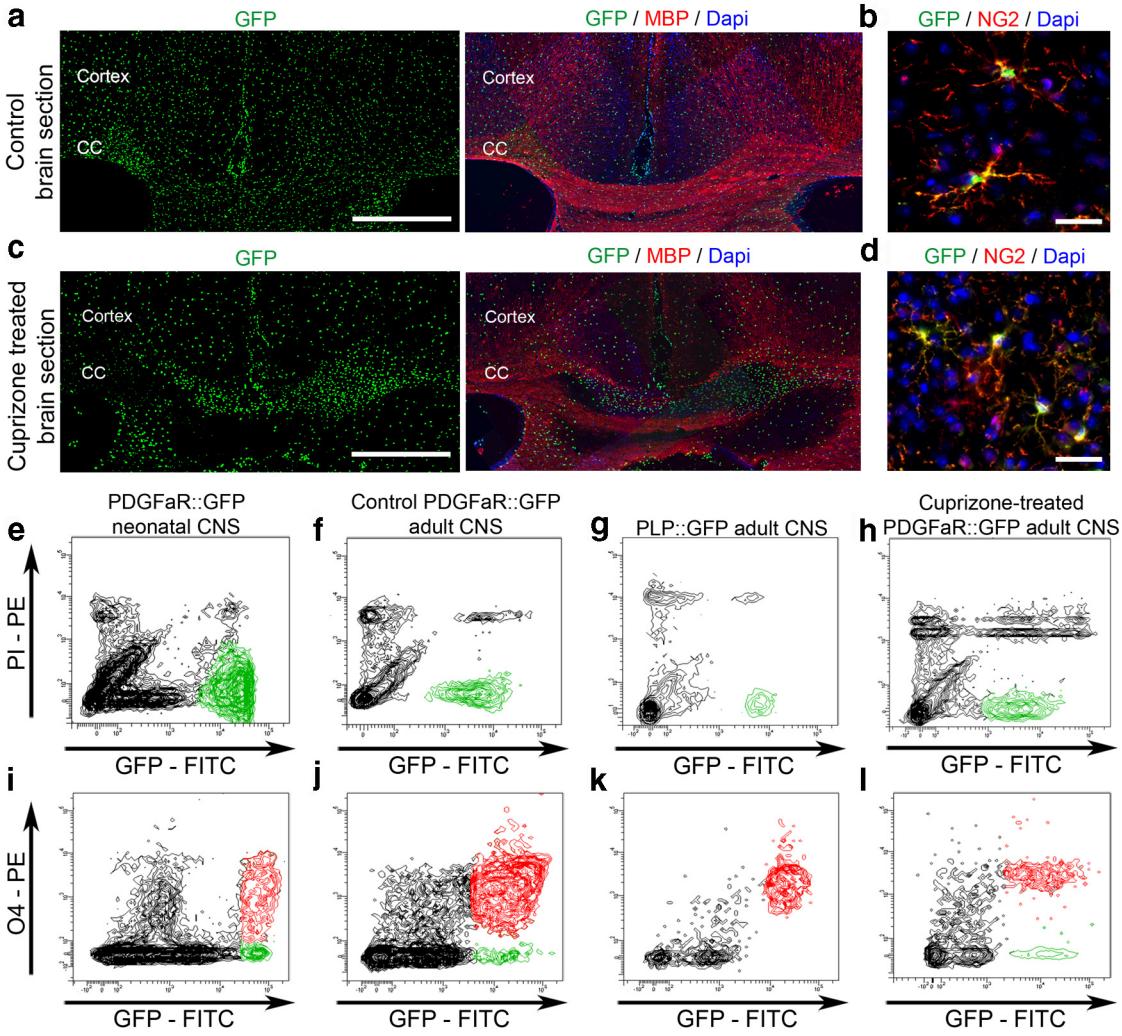

Figure 1. Flow cytometry sorting of OPCs and OLs. ***a***, Coronal section of a control adult *PDGFαR::GFP* brain showing homogeneously distributed GFP-positive aOPCs. Scale bar, 200 μm. ***b***, GFP-positive cells are also expressing NG2. Scale bar, 50 μm. ***c***, Coronal section of a demyelinated brain treated with cuprizone for 5 weeks, showing increased GFP-positive cell density within the demyelinated areas (lack of MBP staining). Scale bar, 200 μm. ***d***, GFP-positive cells expressing NG2 on a cuprizone-treated brain section. Scale bar, 50 μm. ***e***, ***f***, ***h***, Neonatal OPCs (***e***), and adult OPCs from control (***f***) and from demyelinated conditions (***h***) are sorted by flow cytometry from *PDGFαR::GFP* brains. ***g***, Mature OLs are isolated from *PLP-GFP* brains. All sorted cells are GFP positive and PI negative. ***i–l***, Flow cytometry analysis of O4 expression in neonatal OPCs (***i***), adult OPCs from control (***j***), demyelinated brains (***l***) and mature OLs (***k***). CC, Corpus callosum.

biological replicates. Total RNA prepared from each cell type was used to generate labeled RNA, which were hybridized to Agilent whole-mouse-genome microarrays. To validate the data obtained, we first examined genes known to be specific to the oligodendrocyte lineage. Quantitative comparison of gene expression data from nOPCs, aOPCs, and mature OLs distinguished the three cell populations (Fig. 3*a*). For example, NG2 was highly expressed by nOPCs and aOPCs compared with OLs (a 93.1-fold increase in nOPCs, $p < 0.001$; and a 2.74-fold increase in aOPCs, $p < 0.05$). Similar differential expression occurred with PDGFαR (214.6-fold increase in nOPCs, $p < 0.001$; 4.53-fold increase in aOPCs, $p < 0.05$, compared with OLs). Conversely, mRNAs of MBP, myelin-associated oligodendrocyte basic protein (MOBP), and myelin oligodendrocyte glycoprotein (MOG) were more highly expressed in OLs compared with nOPCs (MBP: 4.46-fold increase, $p < 0.001$; MOBP: 25.5-fold increase, $p < 0.01$; MOG: 41.2-fold increase, $p < 0.001$, in OLs compared with nOPCs). However, the expression of these differentiation-associated genes was also significantly greater in aOPCs than in nOPCs (MBP: 4.20-fold increase $p < 0.01$; MOBP: 77.9-fold increase $p < 0.005$; MOG: 43.7-fold increase $p < 0.001$, in aOPCs compared with nOPCs).

Unsupervised hierarchical clustering of all genes revealed that aOPCs and OLs have a gene expression profile more similar to each other than to nOPCs (Fig. 3*b*). Such clustering was not due to the differential expression of genes related to cell division, as the dendrogram pattern was not modified when proliferation and cell cycle-related genes were excluded from the analysis. To identify genes most differentially expressed among the three cell populations, we used Student's *t* test and Benjamini–Hochberg test (cutoff: $p < 0.001$ and $q < 0.03$), which revealed 2361 genes differentially expressed between nOPCs and aOPCs (with fold changes up to 100 for the highly differentially expressed genes) but only 37 genes differentially expressed between aOPCs and OLs (fold changes up to 20 for the highly differentially expressed genes). Thus, nOPCs and aOPCs have distinct gene expression profiles, with aOPCs having a profile that more closely resembles that of OLs.

Gene expression profile of aOPCs reverts to that of nOPCs following demyelination

To examine the activated aOPC transcriptome following demyelination, we isolated aOPCs from 2-month-old *PDGFαR:GFP*

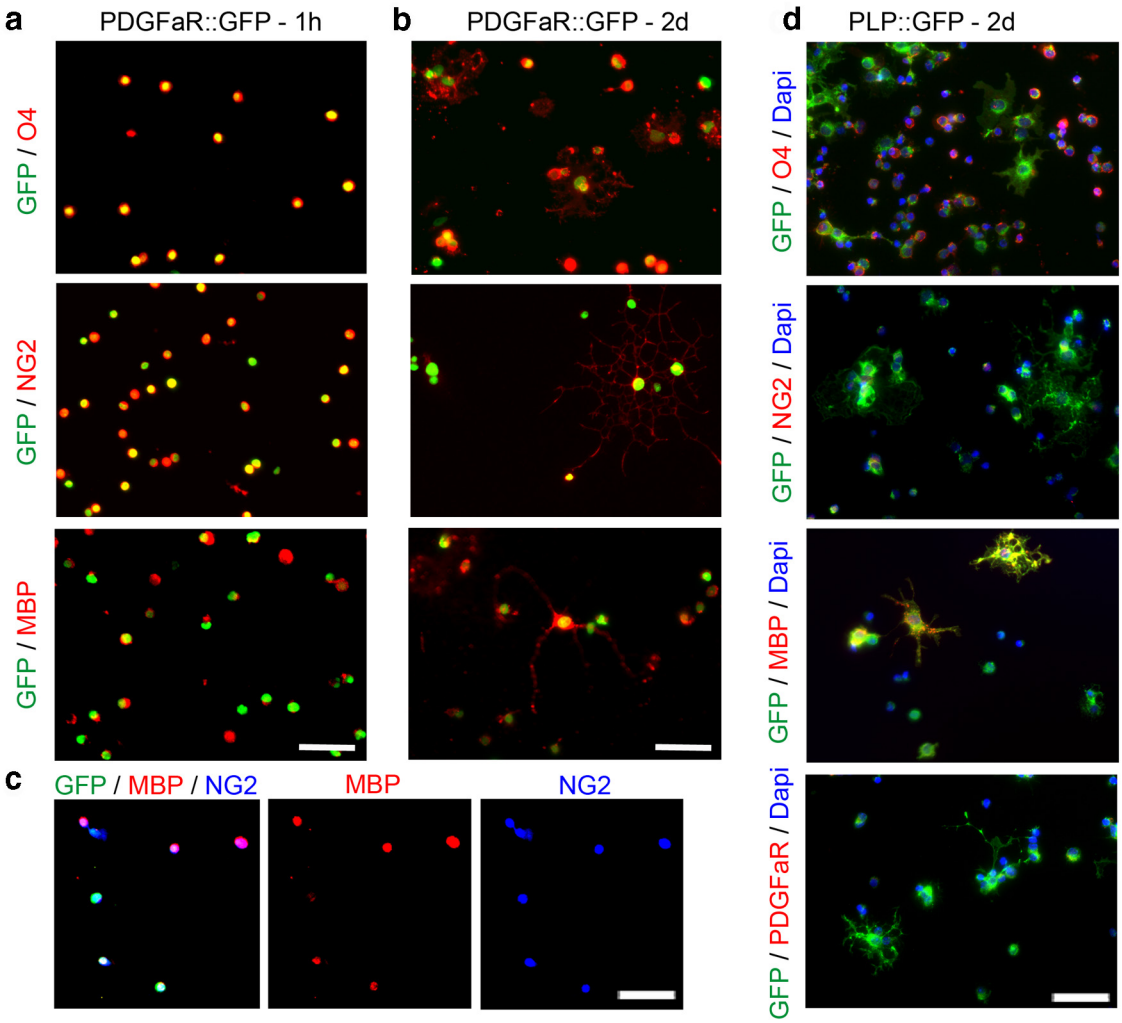

Figure 2. *In vitro* characterization of the sorted cell populations. ***a***, ***b***, Immunolabeling on sorted GFP-positive cells isolated from *PDGFαR::GFP* brains, 60 min after cell platting (***a***) or after 2 d in culture (***b***). Sorted aOPCs express NG2 and O4, as well the mature marker MBP. Scale bar, 50 μm. ***c***, Triple staining with GFP/NG2/MBP. ***d***, Immunolabeling on GFP-positive cells isolated from *PLP-GFP* brains, after 2 d in culture. Only a percentage of sorted aOLs express O4, whereas almost all express MBP. NG2 or PDGFαR expressions are not detected on aOLs. Scale bar, 50 μm.

mice in which demyelination had been induced by feeding them a cuprizone diet (0.2%) for 5 weeks. In initial experiments, we showed low interindividual variability in the extent of demyelination between cuprizone-treated mice, with 93% of them having a demyelinated corpus callosum and areas of demyelination in the cerebral cortex ($n = 23$; Fig. 1*c*; Skripuletz et al., 2008; Koutsoudaki et al., 2009; Silvestroff et al., 2012). We first established that the vast majority of GFP-positive cells coexpressed NG2 *in vivo* (86.1 ± 9.0% in demyelinated slices; Fig. 1*d*). O4 expression by GFP-positive cells, assessed by flow cytometry analysis (Fig 1*h*,*l*), was not significantly different between control and demyelinating conditions (94.9 ± 1.6% and 89.7 ± 3.6%, respectively; Fig. 1*j*,*l*).

Transcriptomic analysis was performed as described above. Initial analysis revealed that aOPCs from demyelinated brains (henceforth described as "activated aOPCs") expressed nOPC-associated genes at higher levels and OL-associated genes at lower levels than aOPCs from normal CNS (henceforth described as "nonactivated aOPCs"). For example, the expression of NG2 was increased 4.2-fold ($p < 0.001$) in activated aOPCs compared with nonactivated OPCs, whereas genes associated with myelination had lower levels of expression [e.g., expression was decreased by 2.6-fold ($p < 0.005$) and 2.8-fold ($p < 0.005$), respectively, for MOBP and MOG expression; Fig. 3*a*]. These demyelination-induced changes in aOPC gene expression are further illustrated by Volcano plot analysis, performed by plotting the fold change (log2 "ratio activated aOPCs/nonactivated aOPCs") of genes that were differentially expressed against their significance (−log10 "*p*"; Fig. 3*c*). Unsupervised hierarchical clustering of the different samples further revealed the distinctive gene expression profiles of activated versus nonactivated aOPCs. The dendrogram showed that activated aOPCs were clustered in a third branch, between nonactivated aOPCs and OLs on one side, and nOPCs on the other (Fig. 3*b*). These results indicate that activated aOPCs have a gene expression pattern that is distinct from that of nonactivated aOPCs, reverting to a pattern of gene expression that more closely resembles that of nOPCs.

Activated aOPCs have increased migration and accelerated differentiation compared with nonactivated aOPCs

To gain insight into the functional changes conferred on aOPCs upon activation, we compared proliferation, survival, migration, and differentiation rates between activated and nonactivated aOPCs in a series of cell culture assays. No differences in either the proportions of proliferative or apoptotic cells were detected (Fig. 4*a*,*b*). Migration rates were quantified using the xCEL-

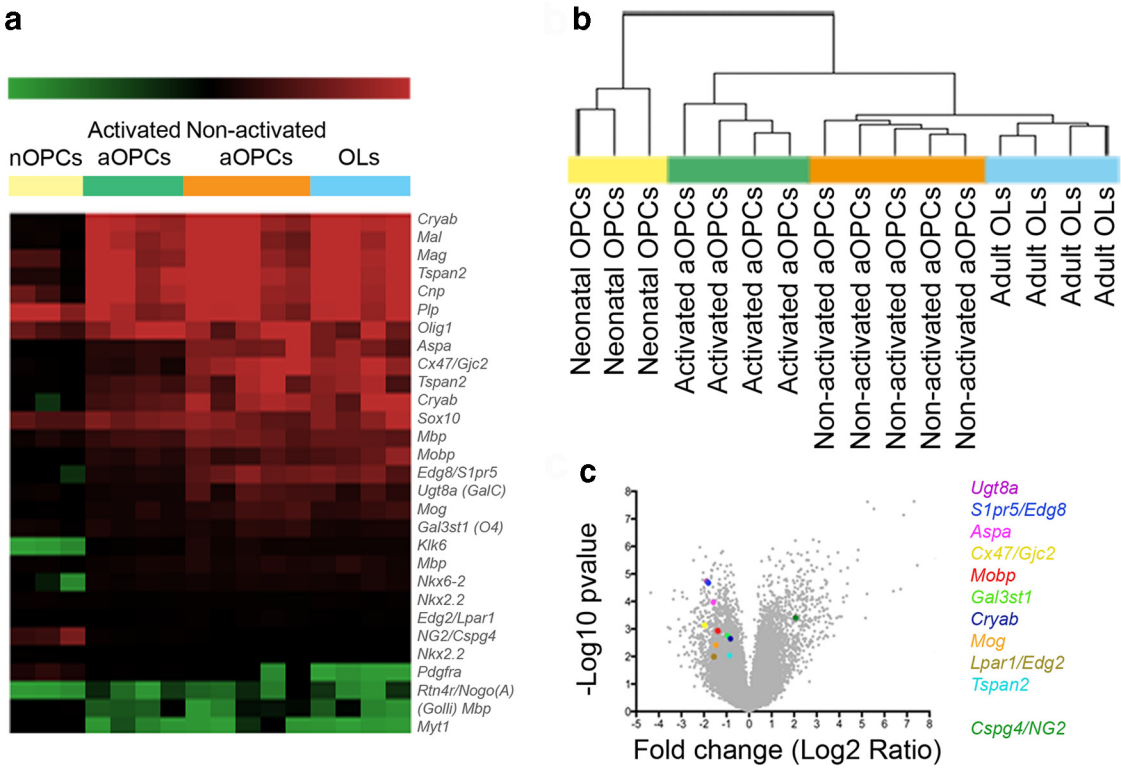

Figure 3. mRNA profile of the sorted populations. ***a***, Microarray analysis restricted to oligodendroglial genes showing the different profiles of each population. ***b***, Hierarchical clustering of all genes (dendogram): each column represents the gene expression of one replicate (Pearson correlation, using Multi-Experiment Viewer). Volcano plot (*x*-axis = Log2 ratio activated vs nonactivated aOPCs; *y*-axis = −Log10 *p* value) shows the changes induced by demyelination in aOPCs, and colored dots point to some known oligodendroglial markers. ***c***, On the right are genes overexpressed, and on the left genes underexpressed by activated aOPCs.

Lingence Migration System wells over 2 d, showing a 1.3-fold increase in migration rate in activated aOPCs compared with nonactivated aOPCs (Fig. 4*c*). Since *in vitro* aOPCs express mature oligodendroglial markers, classifying the stages of differentiation using antigenic markers was not possible, so we therefore used a morphological classification of oligodendroglial development that was adapted from Huang et al. (2011). This analysis revealed that activated aOPCs differentiate more rapidly compared with nonactivated aOPCs (Fig. 4*d*). This faster rate of differentiation of activated aOPCs was similar to the rate of differentiation of nOPCs (Fig. 4*d*).

These results indicate that the changes in gene expression that occur upon demyelination-induced activation conferred on aOPCs increased motility and the rate of differentiation.

Activated aOPCs have increased expression of genes associated with innate immune system function

To identify which changes in gene expression that occur with activation might account for functional changes, we identified all genes significantly differentially expressed between activated and nonactivated aOPCs. This selection was performed using Student's *t* test and Benjamini–Hochberg test (cutoff: $p < 0.001$ and $q < 0.03$; Tables 1, 2). This resulted in the selection of 839 differentially expressed genes, which were then classified according to gene ontology (Fig. 5*a*). We then compared our data with a previously published database of gene expression occurring during remyelination of toxin-induced demyelination of adult rat CNS white matter (Huang et al., 2011), reasoning that genes with differential expression in both isolated activated aOPCs and in remyelinating lesions were likely to have functional significance. Specifically, to identify putative genes responsible for the enhanced migration of activated aOPCs, we compared our activated aOPC profile with genes that had decreased expression in the remyelination model from the stage of 14 d postlesion (dpl), when recruited OPCs are undergoing differentiation, compared with 5 dpl, when OPC recruitment is maximal. One hundred nineteen genes were differentially expressed in both databases (cutoff: $q < 0.05$ used for both databases; Fig. 5*b*,*c*; Table 3). Using Ariadne Genomics-Pathway Studio to identify likely genes interactions within these 119 genes, we selected the following group of 7 interacting genes: *IL1β*, *CCL2*, *P2RY2*, *DDIT3*, *PTK2*, *HSPB2*, and *SMAD7*. Among these seven genes, the expression of *IL1β*, *CCL2*, *P2RY2*, and *DDIT3* was increased, whereas the expression of *PTK2*, *HSPB2*, and *SMAD7* was decreased in activated aOPCs compared with nonactivated aOPCs (Fig. 5*d*). Within the genes with increased expression, we noted the following two genes associated with innate immune system signaling proteins: interleukin-1β [*IL1β*; 1.7-fold increase) and Ccl2 chemokine (*CCL2*, also known as *MCP-1* (monocyte chemoattractant protein 1); 2.4-fold increase]. We confirmed the increased expression of these two genes using qPCR (2.9-fold increase of *IL1β*; 3.5-fold increase of *CCL2*). In contrast, there was no quantitative difference in mRNA levels of *IL1R1* and *CCR2*, the two major receptors of Il1β and Ccl2, respectively (Fig. 5*e*).

Ccl2 expression is increased within areas of cuprizone-induced demyelination

We next asked whether Ccl2 and Il1β were expressed by aOPCs *in vivo* in normal and demyelinated white matter of *PDGFαR:GFP* transgenic mice. By immunohistochemistry, increased Il1β and Ccl2 expression was detected in demyelinated areas, compared with control brain sections (Fig. 6*a*). As the expression of Il1β was

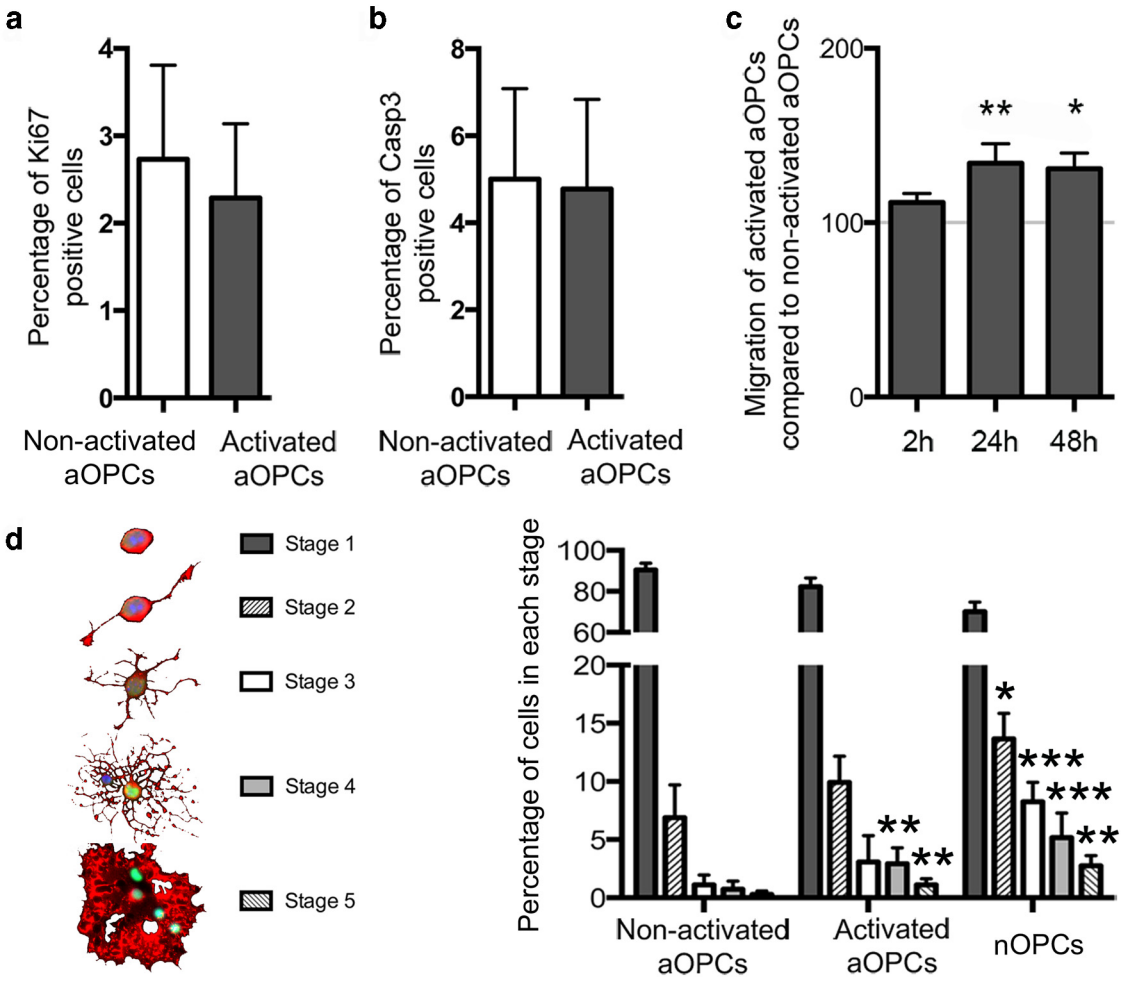

Figure 4. *In vitro* functional changes in activated aOPCs. ***a***, ***b***, After 2 d *in vitro*, the proportions of activated and nonactivated aOPCs undergoing proliferation (***a***) and apoptosis (***b***) are similar. ***c***, *In vitro* vertical migration assessed during a 2 d period, showing at 24 and 48 h a 1.3-fold increased migration of activated aOPCs compared with nonactivated aOPCs ($n = 6$; paired Student's *t* test). Differentiation is assessed using morphological classification (stages 1–5; adapted from Huang et al., 2011; schematic representation on the left). ***d***, After 3 d, activated aOPCs are more differentiated than nonactivated aOPCs, with a higher proportion of cells in stages 4 and 5, a pattern ressembling nOPC differentiation ($n = 3$; paired Student's *t* test, $^{***}p < 0.001$, $^{**}p < 0.005$, $^{*}p < 0.05$).

mostly diffuse, quantification of the proportion aOPCs expressing Il1β in demyelinated tissue was difficult (Fig. 6*b*). The percentage of GFP-positive aOPCs expressing Ccl2 (Fig. 6*b*,*c*) increased from 30.1 ± 6.1% to 79.3 ± 2.0% between control and demyelinated brain areas (Fig. 6*d*).

Il1β and Ccl2 increase adult OPCs migration *in vitro*

To assess the effects of Il1β and Ccl2 on nonactivated aOPCs, cells were cultured with different concentrations of Il1β recombinant protein (2, 5, and 10 ng/ml) or Ccl2 recombinant protein (2, 10, and 20 ng/ml). Proliferation, apoptosis, and differentiation were not altered by Il1β or Ccl2 (data not shown). However, 20 ng/ml Ccl2 caused a significant increase in aOPC migration, which was reversed by the specific Ccr2 receptor antagonist INCB (Fig. 7*a*). Similarly, 5 ng/ml Il1β also caused an increase in aOPC migration, which was repressed by the Il1β receptor antagonist Il1ra (Fig. 7*b*).

Using videomicroscopy, we followed the motion of individual aOPCs over a 24 h period (Fig. 7*c*). This revealed that the addition of Ccl2 and Il1β increased the percentage of motile aOPCs (30.8 ± 2.2%, $p < 0.005$; and 31.3 ± 8.9%, $p < 0.05$, respectively), compared with nontreated cells (12.2 ± 2.9%). Indeed, Ccl2- and Il1β-treated nonactivated aOPCs become as mobile as activated aOPCs [activated aOPCs, 37.0 ± 7.9% ($p < 0.01$), which is not further increased by Ccl2 or Il1β treatment; Fig. 7*c*,*d*]. The chemokinetic effect of neither agent was associated with changes in velocity (mean velocity, 3.7 ± 1.1 mm/week for each condition).

We next showed, using ELISA of the supernatant of cultured aOPCs, that the Ccl2 secretion was significantly greater in activated aOPCs compared with nonactivated OPCs (132.2 ± 42.4 and 67.8 ± 4.9 pg/ml, respectively; $p < 0.05$; Fig. 6*e*). We were unable to detect Il1β in supernatants of either cultured activated or nonactivated OPCs. For this reason, our subsequent studies focused on Ccl2.

These data suggest a model in which aOPCs respond to demyelination by increasing the expression of Ccl2 and (possibly) Il1β, which, by enhancing their motility, enable them to populate areas of demyelination more efficiently.

Overexpression of Ccl2 in aOPCs results in increased migration

To assess whether aOPC migration could be enhanced by increasing the expression of Ccl2, cells were isolated from the brains of *PDGFαR:GFP* mice and transduced with either a lentiviral vector expressing Ccl2 linked to mCherry fluorescent

Table 1. The top 50 genes overexpressed in activated aOPCs compared with nonactivated aOPCs

ID	Symbol	Gene name	Activated aOPCs/non-activated aOPCs ratio	*p* value*	*q* value†
A_51_P363947	*Cdkn1a*	Cyclin-dependent kinase inhibitor 1A (P21)	176.23	1.00E-05	0.003
A_55_P1986296	*Tagln2*	Transgelin 2	46.53	0	0.00031
A_51_P330428	*Eif4ebp1*	Eukaryotic translation initiation factor 4E binding protein 1	38.11	0	0.00018
A_51_P519251	*Nupr1*	Nuclear protein 1	37.6	1.00E-04	0.00758
A_55_P1959748	*Asns*	Asparagine synthetase	35.84	9.00E-04	0.02023
A_66_P106661	*Slc7a1*	Solute carrier family 7 (cationic amino acid transporter, $y+$ system), member 1	28.68	0	0.0019
A_51_P241995	*Col5a3*	Collagen, type V, α3	27.97	0	0.00191
A_55_P1954221	*Emp1*	Epithelial membrane protein 1	20.78	1.00E-05	0.003
A_66_P111562	*Ccnd1*	Cyclin D1	20.53	5.00E-05	0.00567
A_51_P315904	*Gadd45g*	Growth arrest and DNA damage-inducible 45 γ	20.08	1.00E-04	0.00758
A_51_P392687	*Vim*	Vimentin	18.26	0.00021	0.01032
A_51_P352968	*Marcks*	Myristoylated alanine-rich protein kinase C substrate	18.06	0.00013	0.0085
A_51_P390538	*Mpeg1*	Macrophage expressed gene 1	17.13	0.00058	0.01618
A_51_P131408	*Tnfrsf12a*	Tumor necrosis factor receptor superfamily, member 12a	16.75	2.00E-05	0.00343
A_51_P102789	*C1qc*	Complement component 1, q subcomponent, C chain	15.89	0.00032	0.01265
A_52_P1197913	*Gadd45b*	Growth arrest and DNA damage-inducible 45 β	15.34	0	0.0019
A_55_P2033376	*1810041L15Rik*	RIKEN cDNA 1810041L15 gene	13.55	0.00344	0.0421
A_51_P110759	*Slc1a1*	Solute carrier family 1 (neuronal/epithelial high-affinity glutamate transporter, system Xag), member 1	12.9	0.00116	0.02318
A_55_P2064547	*Tuba1c*	Tubulin, α1C	12.28	0.00035	0.01296
A_55_P2068892	*Il6ra*	Interleukin 6 receptor, α	12.03	5.00E-05	0.00545
A_51_P359636	*Lgals3bp*	Lectin, galactoside-binding, soluble, 3 binding protein	12.01	0	0.0019
A_55_P2345853	*3200002M19Rik*	RIKEN cDNA 3200002M19 gene	11.86	6.00E-04	0.01648
A_55_P2165869	*Cebpb*	CCAAT/enhancer binding protein (C/EBP), β	11.7	0.00079	0.01914
A_55_P2121608	*Sox4*	SRY-box containing gene 4	11.43	0	0.0019
A_66_P135173	*9630013A20Rik*	RIKEN cDNA 9630013A20 gene	11.23	0.00038	0.01363
A_55_P2000439	*Ptprz1*	Protein tyrosine phosphatase, receptor type Z, polypeptide 1	11.23	0.00382	0.04504
A_55_P1971599	*Bcan*	Brevican	11.09	0.00013	0.00837
A_51_P246317	*Mt2*	Metallothionein 2	11.03	0.00042	0.01385
A_51_P106059	*Traf4*	TNF receptor-associated factor 4	11.02	0.00198	0.03076
A_55_P2162204	*Kctd15*	Potassium channel tetramerization domain containing 15	10.89	2.00E-05	0.00398
A_55_P2162910	*Rtn1*	Reticulon 1	10.8	0.00015	0.0089
A_55_P2024888	*Ctss*	Cathepsin S	10.75	0.00278	0.03756
A_51_P474459	*Socs3*	Suppressor of cytokine signaling 3	10.67	5.00E-05	0.00575
A_51_P501844	*Cyp26b1*	Cytochrome P450, family 26, subfamily b, polypeptide 1	10.59	0.00127	0.02434
A_55_P2122020	*Klf4*	Kruppel-like factor 4 (gut)	10.32	2.00E-05	0.00381
A_55_P2105858	*Atf5*	Activating transcription factor 5	10.27	0	0.00012
A_66_P126332	*Zfp703*	Zinc finger protein 703	10.12	0.00041	0.01382
A_55_P2121856	*Ier5l*	Immediate early response 5-like	9.93	0.00046	0.01449
A_51_P421140	*Tubb6*	Tubulin, β6	9.87	0.00023	0.01097
A_51_P102789	*C1qc*	Complement component 1, q subcomponent, C chain	9.84	0.00378	0.04483
A_55_P1971963	*Tmem176b*	Transmembrane protein 176B	9.62	0.00278	0.03756
A_51_P258690	*Scrg1*	Scrapie responsive gene 1	9.61	0.00013	0.00835
A_55_P1999902			9.6	4.00E-05	0.00485
A_52_P597634	*Fzd1*	Frizzled homolog 1 (*Drosophila*)	9.59	0.00013	0.00836
A_55_P2098598	*Btg1*	B-cell translocation gene 1, anti-proliferative	9.54	0.00029	0.01189
A_55_P2003541	*Nrcam*	Neuron-glia-CAM-related cell adhesion molecule	9.53	1.00E-05	0.00333
A_65_P19395	*H2-D1*	Histocompatibility 2, D region locus 1	9.12	3.00E-05	0.00436
A_51_P159453	*Serpina3n*	Serine (or cysteine) peptidase inhibitor, clade A, member 3N	9	0.00228	0.0336
A_55_P1953728	*Nes*	Nestin	8.75	0.00016	0.00914
A_51_P502614	*Dusp6*	Dual-specificity phosphatase 6	8.72	1.00E-04	0.00758

*Student's *t* test.

†Benjamini–Hochberg test.

protein (CMV_CCL2-2A-mCherry) or a control vector expressing a myc-tagged DsRed fluorescent protein (CMV_DsRed-Myc). After 4 d in culture, GFP-positive/mCherry-positive and GFP-positive/DsRed-positive cells were FAC sorted and replated, where their individual migrations were followed by videomicroscopy over a 24 h period (Fig. 7*e*). Nontransduced aOPCs and aOPCs transduced with the control lentivirus (aOPCs-DsRed) had similar percentages of motile cells (19.9 ± 3.0% and 19.3 ± 3.0%, respectively), while the aOPCs transduced with the CMV_CCL2-2A-mCherry lentiviral vector (aOPCs-Ccl2) had a significantly increased percentage of motile cells (39.8 ± 3.7%; $p < 0.05$; Fig. 7*f*).

We next asked whether aOPCs transduced to express Ccl2 would exhibit enhanced migration following transplantation

Table 2. The top 50 genes overexpressed in nonactivated aOPCs compared with activated aOPCs

ID	Symbol	Gene name	Nonactivated aOPCs/activated aOPCs ratio	*p* value*	*q* value†
A_52_P373694	*Jph4*	Junctophilin 4	20.00	1.00E-05	0.00278
A_52_P540434	*Ppp1cc*	Protein phosphatase 1, catalytic subunit, γ isoform	12.50	0.00156	0.02709
A_55_P2146520	*Carns1*	Carnosine synthase 1	11.11	0.00163	0.02758
A_55_P1984655	*Smtnl2*	Smoothelin-like 2	11.11	0.0016	0.02743
A_55_P1955869	*Gm9315*	Predicted gene 9315	10.00	9.00E-05	0.00734
A_51_P105927	*Rasl12*	RAS-like, family 12	10.00	4.00E-05	0.00486
A_66_P122613	*9630009A06Rik*	RIKEN cDNA 9630009A06 gene	9.09	0.00516	0.05202
A_55_P2044389	*Kif6*	Kinesin family member 6	9.09	0.00013	0.00842
A_51_P246166	*Expi*	Extracellular proteinase inhibitor	8.33	0.00201	0.03104
A_51_P348433	*Rasal1*	RAS protein activator like 1 (GAP1 like)	8.33	0.00072	0.0182
A_55_P2148624	*Gpr61*	G-protein-coupled receptor 61	7.69	1.00E-05	0.00306
A_55_P1996674	*Itih3*	Inter-α trypsin inhibitor, heavy chain 3	7.69	0.00061	0.0166
A_55_P1959485	*LOC634933*		7.69	6.00E-05	0.00643
A_55_P2011286	*Hopx*	HOP homeobox	7.14	0.00218	0.03261
A_55_P2149942	*Ninj2*	Ninjurin 2	7.14	8.00E-04	0.01926
A_55_P2005859	*Fn3k*	Fructosamine 3 kinase	6.67	0.00371	0.04446
A_55_P2042923	*Sgk2*	Serum/glucocorticoid-regulated kinase 2	6.67	4.00E-05	0.00494
A_55_P2243883	*B230117O15Rik*	RIKEN cDNA B230117O15 gene	6.25	0.00021	0.01051
A_51_P285077	*Hhatl*	Hedgehog acyltransferase-like	6.25	0.00178	0.02897
A_51_P430973	*Paqr7*	Progestin and adipoQ receptor family member VII	6.25	0.00508	0.05151
A_51_P200561	*4930506M07Rik*	RIKEN cDNA 4930506M07 gene	5.88	0.00045	0.01418
A_66_P114381	*Ypel2*	Yippee-like 2 (*Drosophila*)	5.88	0.00195	0.03047
A_55_P2268022	*9330199G10Rik*	RIKEN cDNA 9330199G10 gene	5.56	0.0092	0.07041
A_55_P2006525	*Adamtsl4*	ADAMTS-like 4	5.56	0	0.0019
A_52_P559545	*Cercam*	Cerebral endothelial cell adhesion molecule	5.56	0.00177	0.02879
A_51_P316553	*Kdr*	Kinase insert domain protein receptor	5.56	0.00032	0.01261
A_55_P2012430	*LOC100045251*		5.56	0.00176	0.02871
A_55_P2142072	*Synj2*	Synaptojanin 2	5.56	0.00098	0.02134
A_55_P2039606			5.56	0.00055	0.01597
A_55_P2022870			5.56	0.00254	0.03577
A_55_P2076994	*Defa-rs10*	Defensin-α-related sequence 10	5.26	0.00716	0.06191
A_55_P2004159	*LOC100039646*		5.26	0.00053	0.0156
A_55_P1983999	*Pppde2*	PPPDE peptidase domain containing 2	5.26	0.00013	0.00857
A_51_P104710	*Sspo*	SCO-spondin	5.26	0.00986	0.07278
A_55_P1984976	*Wnt5b*	Wingless-related MMTV integration site 5B	5.26	0.00087	0.02004
A_55_P2121352	*Cdk5*	Cyclin-dependent kinase 5	5.00	0.00078	0.0191
A_55_P2227321	*Ptprd*	Protein tyrosine phosphatase, receptor type, D	5.00	0.00028	0.01178
A_52_P563825	*B3galt1*	UDP-Gal:βGlcNAc β 1,3-galactosyltransferase, polypeptide 1	4.76	0.00016	0.00898
A_55_P2131954	*Gm2590*	Predicted gene 2590	4.76	0.00137	0.02533
A_52_P376169	*Lypd6*	LY6/PLAUR domain containing 6	4.76	0.00818	0.06634
A_55_P2042356	*Rftn1*	Raftlin lipid raft linker 1	4.76	0.00105	0.02213
A_52_P493477	*Serpinb1c*	Serine (or cysteine) peptidase inhibitor, clade B, member 1c	4.76	1.00E-04	0.00761
A_51_P112762	*Slc5a3*	Solute carrier family 5 (inositol transporters), member 3	4.76	0.001	0.02155
A_55_P1954680	*B230206H07Rik*	RIKEN cDNA B230206H07 gene	4.55	0.00136	0.02528
A_55_P2102515	*Daam1*	Disheveled associated activator of morphogenesis 1	4.55	0.00049	0.01505
A_51_P349495	*Mboat1*	Membrane-bound *O*-acyltransferase domain containing 1	4.55	0.00347	0.04233
A_55_P1991164	*Mlc1*	Megalencephalic leukoencephalopathy with subcortical cysts 1 homolog (human)	4.55	0.00112	0.02296
A_52_P497188	*Prrg1*	Proline-rich Gla (G-carboxyglutamic acid) 1	4.55	0	0.0019
A_55_P2088965	*Scarb1*	Scavenger receptor class B, member 1	4.55	0.00836	0.06713
A_55_P2121165	*Tmeff1*	Transmembrane protein with EGF-like and two follistatin-like domains 1	4.55	0.00116	0.02318

*Student's *t* test.

†Benjamini–Hochberg test.

into the neonatal mouse brain. Since we were unable to obtain sufficient numbers of transduced primary aOPCs for transplantation, we instead used the CG4 cell line that reliably mimics the behavior of primary OPCs following transplantation (Franklin et al., 1995). Approximately 80% of the CG4 cells were transduced at 3 d postinfection with increased *CCL2* detected by qPCR (Fig. 8*c*), allowing us to sort mCherry-positive or DsRed-positive cells, and to graft these transduced cells into the corpus callosum of neonatal *PDGFαR:GFP* mouse pups (Fig. 8*a*,*d*). We confirmed that CG4 cells were not affected by lentivirus transduction: transduced or nontransduced CG4 cells are immature progenitors, expressing PDGFαR and O4, but not MBP (Fig. 8*b*). We have also checked that nontransduced CG4 cells, as well as CG4 cells transduced with control or Ccl2_mCherry lentivirus, express Ccr2 (data not shown). No difference in the maximal distance of migration was observed between CG4 cells transduced with the control lentivirus (CG4-DsRed) and CG4 cells expressing Ccl2 (CG4-Ccl2) at 40 h after grafting (Fig. 8*e*). However, a significantly increased number of CG4-Ccl2 cells had migrated from the site of injection compared with the

a Genes differentially expressed in activated and non-activated aOPCs:

GO	Number of genes	pvalue
Transport	117	4.11×10^{-12}
Regulation of transcription	120	7.36×10^{-11}
Anti-apoptosis	29	7.16×10^{-10}
Nervous system development	43	5.32×10^{-9}
Cell adhesion	54	8.42×10^{-9}
Cell cycle	47	1.37×10^{-8}
Myelination	13	1.64×10^{-8}
Negative regulation of apoptosis	27	1.10×10^{-7}
Cell differentiation	53	1.14×10^{-7}
Positive regulation of transcription	24	2.27×10^{-7}

b Genes differentially expressed in the 2 databases:

GO	Number of genes	pvalue
Regulation of cellular process	76	1.45×10^{-8}
Regulation of cell proliferation	26	1.78×10^{-5}
Leukocyte migration	4	4.78×10^{-5}
Regulation of biological process	43	4.83×10^{-5}
Regulation of cell death and cell cycle	26	5.94×10^{-5}
Cell migration	10	8.09×10^{-5}
Regulation of sequence-specific DNA binding transcription factor activity	7	2.14×10^{-4}
Positive regulation of transport	7	2.21×10^{-4}
Regulation of nervous system development	10	4.85×10^{-4}
Receptor binding	13	7.07×10^{-4}

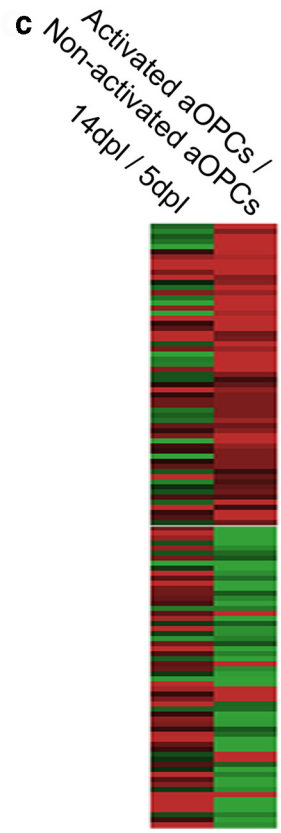

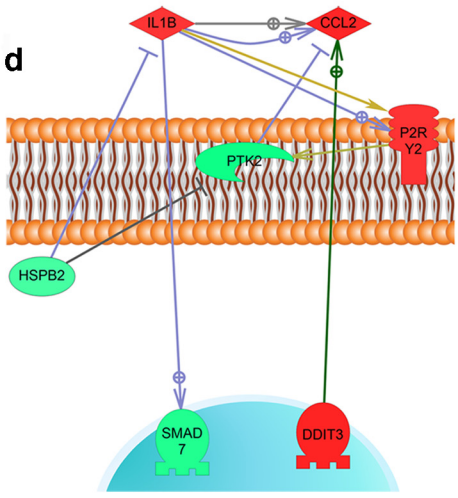

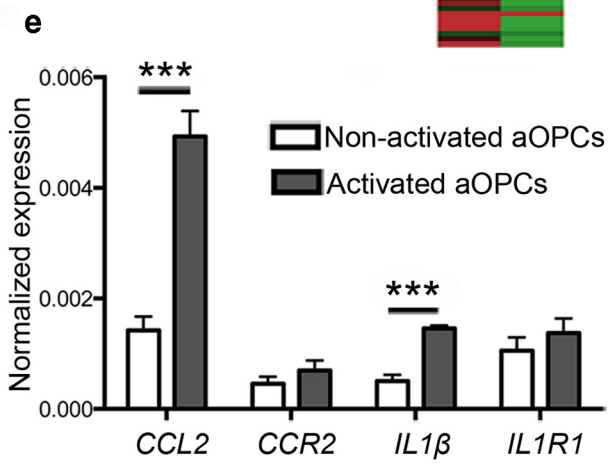

Figure 5. Biostatistical analysis to identify genes of interest. ***a***, Gene ontology performed on GOrilla software for all genes differentially expressed between activated aOPCs and nonactivated aOPCs. ***b***, Gene ontology for genes differentially expressed in activated aOPCs versus those in the nonactivated aOPC database and in the reported early repair database of caudal cerebellar peduncle (CCP) lesions comparing 14 versus 5 dpl. ***c***, Representation of the 119 genes differentially expressed in both databases. ***d***, Identification of a group of seven interacting genes, using Ariadne Genomics–Pathway Studio. ***e***, qPCR detection of *CCL2*, *CCR2*, *IL1β*, and *IL1R1* on activated aOPCs and nonactivated aOPCs. qPCR showing *CCL2* and *IL1β* expression in activated aOPCs ($n = 4$; Student's *t* test, $^{***}p < 0.001$).

control CG4-DsRed (Fig. 8*f*), whereas proliferation rate was similar (Fig. 8*g*).

Ccl2 is expressed within active MS plaque OPCs

We analyzed Ccl2 expression within active regions of MS plaques (i.e., either active plaques or the active border of chronic lesions; see lesion classification in Materials and Methods), and within chronic lesions or NAWM. OPCs were identified by nuclear Olig1 staining. Within active areas, 3–5% of OPCs expressed Ccl2 (Fig. 9*a*,*b*,*e*), whereas only 1–2% were detected in chronic lesions and NAWM (Fig. 9*c*,*d*). Quantification was performed by comparing each MS lesion to adjacent NAWM of the same size (see Materials and Methods). In active MS plaques and the active border of chronic plaques, a 2.4- and 1.7-fold increase of Ccl2-expressing OPCs was detected. In contrast, within chronic plaques, no significant difference was detected (Fig. 9*f*).

Discussion

Using a microarray screen on purified populations of cells of the oligodendroglial lineage, we have been able to specifically analyze the aOPC population and gain insights into intrinsic changes distinguishing demyelination (i.e., distinguishing activated aOPCs from nonactivated aOPCs). We first demonstrated that aOPCs have a more mature transcriptome than nOPCs. These results corroborate previous reports showing that adult O4-positive cells have higher levels of transcripts for myelin genes

Table 3. The 119 genes differentially expressed in both databases

Probe ID illumina	Gene symbol	Fold change in activated aOPC/ nonactivated aOPC ratio	FDR-activated aOPC/ nonactivated aOPC ratio	Fold change 14 dpl/5 dpl ratio	FDR 14 dpl/5 dpl ratio
ILMN_51219	*Mt3*	1.161	0.027	1.796	0.001
ILMN_53363	*Gpd1*	0.970	0.011	1.496	0.001
ILMN_52937	*Nupr1*	5.233	0.000	0.985	0.023
ILMN_59954	*Fxyd6*	2.061	0.005	2.297	0.000
ILMN_58714	*Slc25a29*	0.574	0.049	0.612	0.006
ILMN_64674	*Crip2*	2.135	0.000	1.715	0.000
ILMN_58852	*Nr4a2*	1.105	0.031	0.436	0.005
ILMN_64905	*RGD1311433*	0.557	0.045	0.340	0.003
ILMN_53779	*Mpg*	0.776	0.034	0.343	0.010
ILMN_53158	*RGD1308093*	0.007	0.033	0.371	0.009
ILMN_68876	*NA*	0.030	0.047	0.421	0.009
ILMN_48674	*Fzd1*	3.262	0.000	0.423	0.040
ILMN_49747	*Cirbp*	1.768	0.006	0.451	0.033
ILMN_60518	*Timp3*	2.659	0.002	0.461	0.005
ILMN_66452	*Phlda1*	1.194	0.003	0.519	0.003
ILMN_69826	*Tnfrsf12a*	4.066	0.000	0.690	0.002
ILMN_63705	*Gadd45a*	2.373	0.001	0.759	0.003
ILMN_53681	*RGD1561238*	0.638	0.001	0.791	0.001
ILMN_57274	*Ngfr*	0.871	0.040	0.855	0.009
ILMN_53094	*NA*	1.256	0.004	0.875	0.003
ILMN_51692	*Hbegf*	1.236	0.009	0.954	0.002
ILMN_54579	*Cspg4*	2.057	0.001	0.964	0.006
ILMN_49640	*Ddit4*	1.220	0.007	1.059	0.014
ILMN_66374	*Lmo4*	2.720	0.000	1.073	0.001
ILMN_47800	*Fabp7*	1.585	0.010	1.152	0.000
ILMN_52596	*Col1a2*	1.394	0.004	1.197	0.020
ILMN_56986	*Scg3*	0.834	0.014	1.535	0.001
ILMN_52684	*Col5a3*	4.806	0.000	1.601	0.000
ILMN_55428	*Csrp2*	1.042	0.012	1.993	0.002
ILMN_58726	*Gas6*	0.885	0.011	2.400	0.000
ILMN_69972	*Sparcl1*	0.518	0.034	2.517	0.011
ILMN_67000	*NA*	0.921	0.021	0.876	0.005
ILMN_70091	*Lipa*	−1.234	0.008	−0.577	0.005
ILMN_54243	*Birc2*	−1.350	0.009	−1.605	0.000
ILMN_52565	*Myadm*	−1.113	0.049	−0.971	0.001
ILMN_57271	*Faim*	−0.764	0.033	−0.765	0.000
ILMN_63415	*Nfe2l2*	−0.652	0.020	−0.593	0.014
ILMN_58795	*Atp6ap2*	−0.659	0.042	−0.517	0.000
ILMN_59859	*Arfgef2*	−1.117	0.044	−0.496	0.022
ILMN_48347	*Xpo1*	−0.800	0.028	−0.468	0.030
ILMN_51090	*RGD1561318*	−0.985	0.003	−0.465	0.001
ILMN_52394	*Gyg1*	−0.893	0.016	−0.385	0.006
ILMN_57554	*Tmem49*	−0.887	0.006	−0.360	0.020
ILMN_55052	*Fpgt*	−0.568	0.029	−0.358	0.008
ILMN_51657	*Bmp2k*	−1.018	0.004	−0.354	0.042
ILMN_62852	*M6prbp1*	−0.982	0.023	−0.353	0.032
ILMN_55477	*RGD1561318*	−1.285	0.010	−0.314	0.023
ILMN_65955	*Slc26a11*	−1.416	0.019	−0.286	0.012
ILMN_69380	*Hapln2*	−0.787	0.029	−0.913	0.018
ILMN_53575	*LOC100362769*	0.343	0.010	−0.499	0.036
ILMN_54331	*Slc38a1*	2.431	0.000	−0.600	0.002
ILMN_61673	*P2ry2*	1.746	0.047	−1.288	0.001
ILMN_69830	*Ddit3*	2.473	0.001	−0.655	0.001
ILMN_70092	*Arf6*	1.550	0.004	−0.556	0.001
ILMN_63004	*NA*	2.659	0.031	−0.713	0.006
ILMN_58897	*Emb*	1.531	0.035	−1.498	0.001
ILMN_56900	*Acaa2*	1.605	0.001	−0.624	0.036
ILMN_55502	*C1qc*	3.990	0.001	−0.711	0.048
ILMN_50644	*Il1b*	1.669	0.037	−2.340	0.003
ILMN_68242	*Ccl2*	2.396	0.001	−1.441	0.007
ILMN_60683	*RGD1309759*	1.394	0.010	−1.179	0.000
ILMN_48844	*Fam3c*	1.370	0.021	−1.063	0.001
ILMN_52928	*Anxa5*	1.065	0.005	−0.810	0.003
ILMN_60037	*Lgals3bp*	3.586	0.000	−0.803	0.008
ILMN_59873	*Sdad1*	0.616	0.023	−0.791	0.003
ILMN_58534	*Impa2*	1.511	0.050	−0.759	0.012
ILMN_67102	*Naprt1*	1.261	0.018	−0.700	0.003
ILMN_62651	*Eif4ebp1*	5.252	0.000	−0.698	0.005
ILMN_66666	*NA*	1.732	0.012	−0.591	0.037
ILMN_53677	*Scamp2*	0.477	0.050	−0.537	0.005
ILMN_60223	*Gsto1*	2.157	0.003	−0.524	0.002
ILMN_50677	*Sh3bp4*	0.903	0.039	−0.504	0.036
ILMN_61212	*Mad2l1bp*	0.509	0.046	−0.503	0.009
ILMN_51505	*Txnrd1*	0.862	0.014	−0.415	0.030
ILMN_50573	*Serp1*	0.781	0.021	−0.289	0.036
ILMN_61404	*Cst3*	1.121	0.011	−0.231	0.046
ILMN_48324	*Sbds*	−0.601	0.048	0.460	0.010
ILMN_61670	*Carhsp1*	−0.680	0.015	0.489	0.008
ILMN_48913	*Hspb2*	−0.503	0.043	0.584	0.009
ILMN_63175	*Abca2*	−1.737	0.007	0.597	0.020
ILMN_58653	*Cldnd1*	−0.550	0.039	0.600	0.000
ILMN_53618	*Clcn2*	−1.377	0.011	0.611	0.006
ILMN_56148	*Atrn*	−0.540	0.039	0.638	0.006
ILMN_54730	*Pomgnt1*	−0.972	0.008	0.673	0.001
ILMN_57175	*Phlpp1*	−0.985	0.013	0.746	0.002
ILMN_55608	*Arl2*	−0.860	0.024	0.786	0.000
ILMN_63002	*Apln*	−1.388	0.005	0.816	0.001
ILMN_53865	*NA*	−0.659	0.050	0.883	0.000
ILMN_55899	*Fntb*	−1.130	0.021	0.892	0.001
ILMN_57086	*Slc44a1*	−0.803	0.010	1.022	0.002
ILMN_56690	*Prkcz*	−1.349	0.003	1.050	0.015
ILMN_60295	*Myo1d*	−1.772	0.029	1.133	0.000
ILMN_47781	*Cdc42ep2*	−1.084	0.010	1.256	0.000
ILMN_56537	*Tppp3*	−1.099	0.010	1.316	0.000
ILMN_48166	*Aldh1a1*	−1.820	0.009	1.630	0.030
ILMN_61133	*Jam3*	−1.128	0.003	2.144	0.000
ILMN_65657	*Pafah1b2*	−1.285	0.013	0.286	0.026
ILMN_66755	*NA*	−1.007	0.005	0.289	0.013
ILMN_57177	*Ppp2r5b*	−0.544	0.034	0.299	0.040
ILMN_53817	*Rbbp6*	−1.053	0.050	0.315	0.020
ILMN_56707	*Zfp354a*	−0.983	0.019	0.343	0.012
ILMN_64783	*Ermp1*	−1.007	0.005	0.387	0.044
ILMN_55879	*Klhl2*	−0.799	0.012	0.417	0.014
ILMN_48256	*Smad7*	−1.237	0.002	0.465	0.004
ILMN_52620	*Fam115a*	−0.799	0.029	0.493	0.035
ILMN_52044	*LOC100365024*	−1.130	0.028	0.498	0.034
ILMN_68931	*Ptk2*	−1.832	0.021	0.537	0.042
ILMN_63713	*Epdr1*	−0.836	0.010	0.547	0.036
ILMN_58939	*Lrig3*	−0.856	0.023	0.577	0.019
ILMN_55683	*NA*	−0.802	0.013	0.654	0.010
ILMN_67298	*Thra_v2*	−1.409	0.019	0.733	0.020
ILMN_56830	*Znf536*	−0.894	0.014	0.968	0.002
ILMN_69891	*Prkcq*	−0.683	0.021	0.976	0.000
ILMN_60293	*Frmd8*	−0.913	0.006	0.987	0.000
ILMN_161522	*Tmem98*	−0.860	0.021	0.993	0.002
ILMN_59078	*Tmprss5*	−1.121	0.010	1.181	0.000
ILMN_56185	*Tmem98*	−1.482	0.002	1.233	0.000
ILMN_61041	*Bpgm*	−0.887	0.015	1.369	0.000
ILMN_64748	*Ndrg2*	−0.637	0.015	1.764	0.024

Ratios and *q* values by Benjamini–Hochberg test in both databases. FDR, False discovery rate.

compared with neonatal O4-positive cells (Lin et al., 2009). It has been suggested that myelin-associated proteins inhibit OPC differentiation, in part, by suppressing the expression of Nkx2.2, which could explain the maintenance of undifferentiated aOPCs

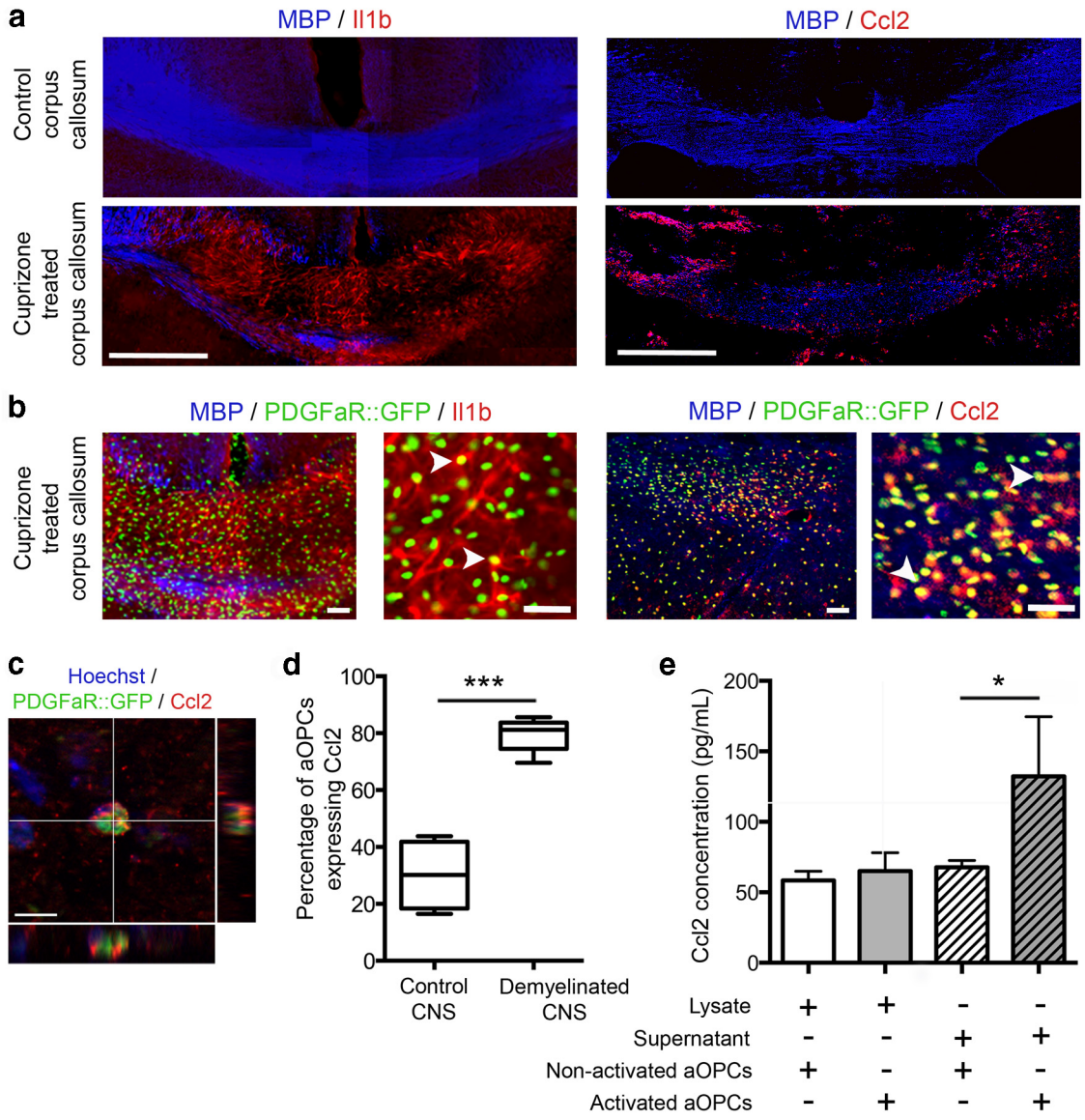

Figure 6. *In vivo* Il1β and Ccl2 expression by aOPCs in control and cuprizone-treated *PDGFαR:GFP* adult mice. ***a***, Immunostaining on coronal brain sections of control and cuprizone-treated *PDGFαR::GFP* adult mice showing increased numbers of aOPCs (GFP-positive cells) in the demyelinated area (corpus callosum) associated with increased expression of Il1β and Ccl2. Scale bar, 200 μm. ***b***, Higher-magnification image showing GFP-positive aOPCs expressing Il1β and Ccl2 (white arrowheads). Scale bar, 50 μm. ***c***, A GFP-positive cell expressing Ccl2. Scale bar, 10 μm. ***d***, Quantification of the percentage of aOPCS expressing Ccl2 showing a 2.5-fold increase after demyelination ($n = 5$; Student's *t* test $^{***}p < 0.001$). ***e***, ELISA performed on lysates and supernatants of purified aOPCs from control and demyelinated brains showing a twofold increase of Ccl2 secretion by activated aOPCs compared with nonactivated aOPCs (Student's *t* test, $^{*}p < 0.05$).

in adult brains (Robinson and Miller, 1999; Syed et al., 2008). This mature pattern of aOPC gene expression is also evident from a comparison with the mRNA profile of OLs sorted from PLP: GFP transgenic lines. A much lower number of genes (37 genes) are differentially regulated between the two cell types, compared with the high number of genes (2361 genes) differentially regulated between aOPCs and nOPCs. A major issue for the microarray data validation was to ascertain that the sorted cell populations from adult *PLP-GFP* and *PDGFαR:GFP* brains corresponded to populations of OLs and OPCs, respectively. Since aOPCs express PLP transcripts, one caveat might have been the possibility that sorting from adult *PLP-GFP* transgenic lines results in the isolation of a mixed population of OLs and aOPCs. This possibility was ruled out by the fact that sorted *PLP-GFP* OLs do not express immature markers NG2 or PDGFαR (which are expressed by aOPCs). Furthermore, as we could not rule out that some GFP-expressing cells in the adult brain of *PDGFαR:GFP* mice were already differentiated oligodendrocytes, while retaining GFP expression, we assessed the *in vivo* expression of NG2, a progenitor marker. Whereas 91.7% of all GFP-positive cells express NG2, some low GFP expressing cells were NG2 negative, suggesting that these were differentiating cells. We then confirmed that all sorted cells expressed NG2.

Sorted aOPCs express MBP, a marker of mature oligodendrocytes. Although we cannot rule out that MBP expression is "artificially" induced by the cellular stress related to the isolation procedure, these data are in line with the microarray data, but also with previously published data (Li et al., 2002; Ruffini et al., 2004; Lin et al., 2009), showing the expression of different mature

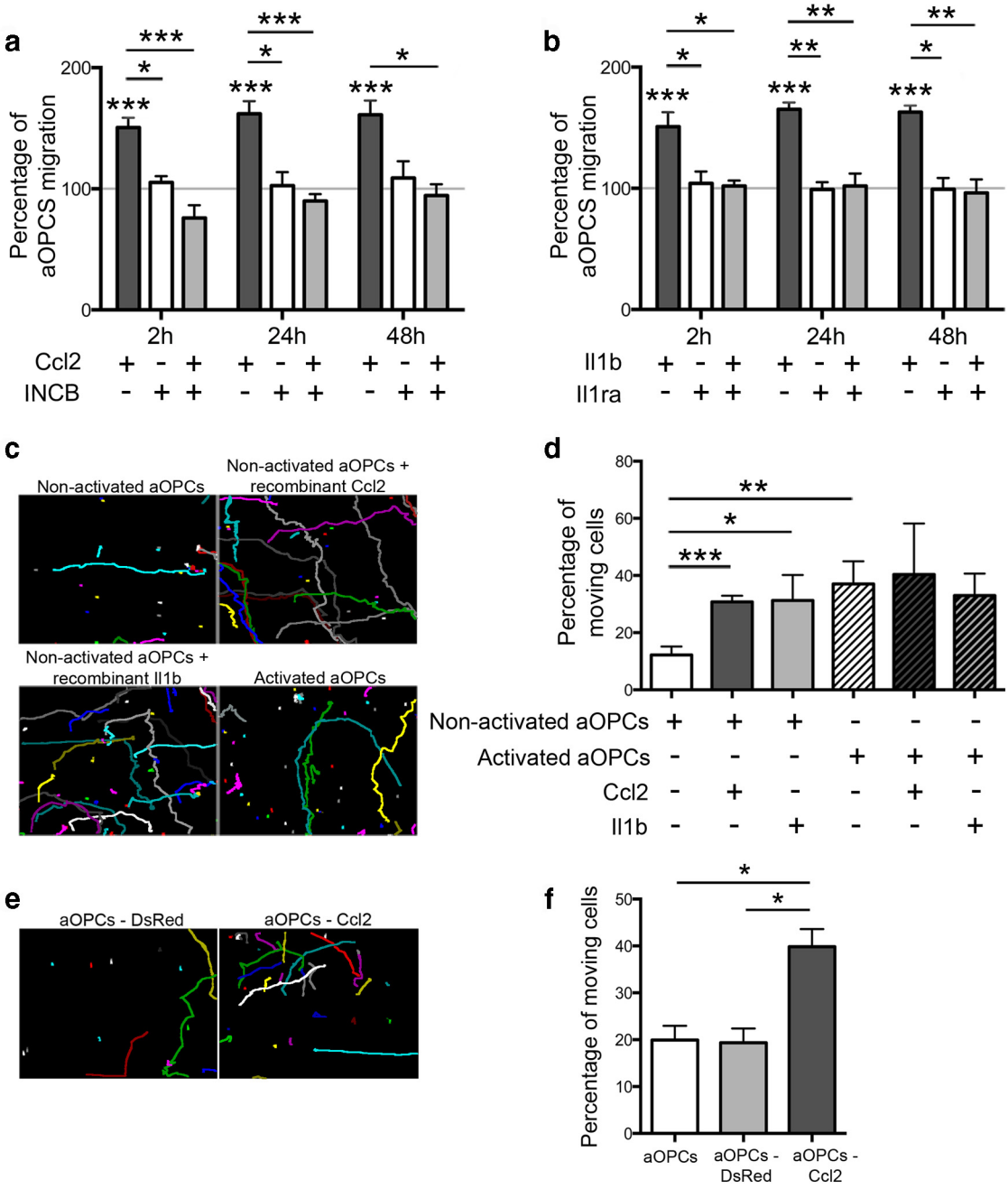

Figure 7. Influence of Il1β and Ccl2 on aOPC migration *in vitro*. ***a***, ***b***, Soluble Ccl2 (20 ng/ml) and Il1β (5 ng/ml) increase aOPC migration, compared with control in a vertical migration system. This effect is blocked by the respective antagonists INCB (for Ccl2, 8 μM) and Il1ra1 (for Il1β, 200 ng/ml; Student's *t* test, $^{*}p < 0.01$, $^{**}p < 0.005$, and $^{***}p < 0.001$). ***c***, ***d***, Horizontal migration assessed by video microscopy (each colored spot represents a single cell track, ***c***) showing that nonactivated aOPCs treated by soluble Ccl2 or Il1β become as mobile as activated aOPCs (treated or not with Ccl2 or Il1β; ***d***). ***e***, ***f***, A similar increase is induced by lentiviral-mediated overexpression of Ccl2 (aOPCs-Ccl2) compared with control vector (aOPCs-DsRed; $n = 3$; Student's *t* test, $^{*}p < 0.05$, $^{**}p < 0.01$, and $^{***}p < 0.002$).

markers by OPCs in the adult CNS. Nevertheless, we were unable to detect MBP expression on *PDGFαR::GFP*-positive cells *in vivo*, suggesting the low expression of the protein.

Using the cuprizone model, we showed that aOPCs revert to a more immature mRNA expression profile after demyelination and acquire new capacities. To further validate that GFP-positive cells were corresponding to adult OPCs in demyelinated CNS, we have assessed *in vivo* that, as under control conditions, the GFP-positive cells expressed NG2. In addition, although we cannot exclude the idea that a small proportion of activated cells are newly generated from the germinal zone of cuprizone-treated brains, GFP-positive cells were disseminated within the whole white matter of cuprizone-treated mice, suggesting that sorted cells were mostly "local" aOPCs rather than aOPCs newly generated from activated neural stem cells.

Several previous studies have analyzed gene expression profiles in CNS demyelinating lesions, but none focused on a single cell population (Jurevics et al., 2002; Huang et al., 2011). Using a rat model of toxin-induced demyelination, Fancy et al., 2009 reported that ~50 transcription factor-encoding genes show dynamic expression during remyelination including the Wnt pathway mediator Tcf4, leading to the identification of a major

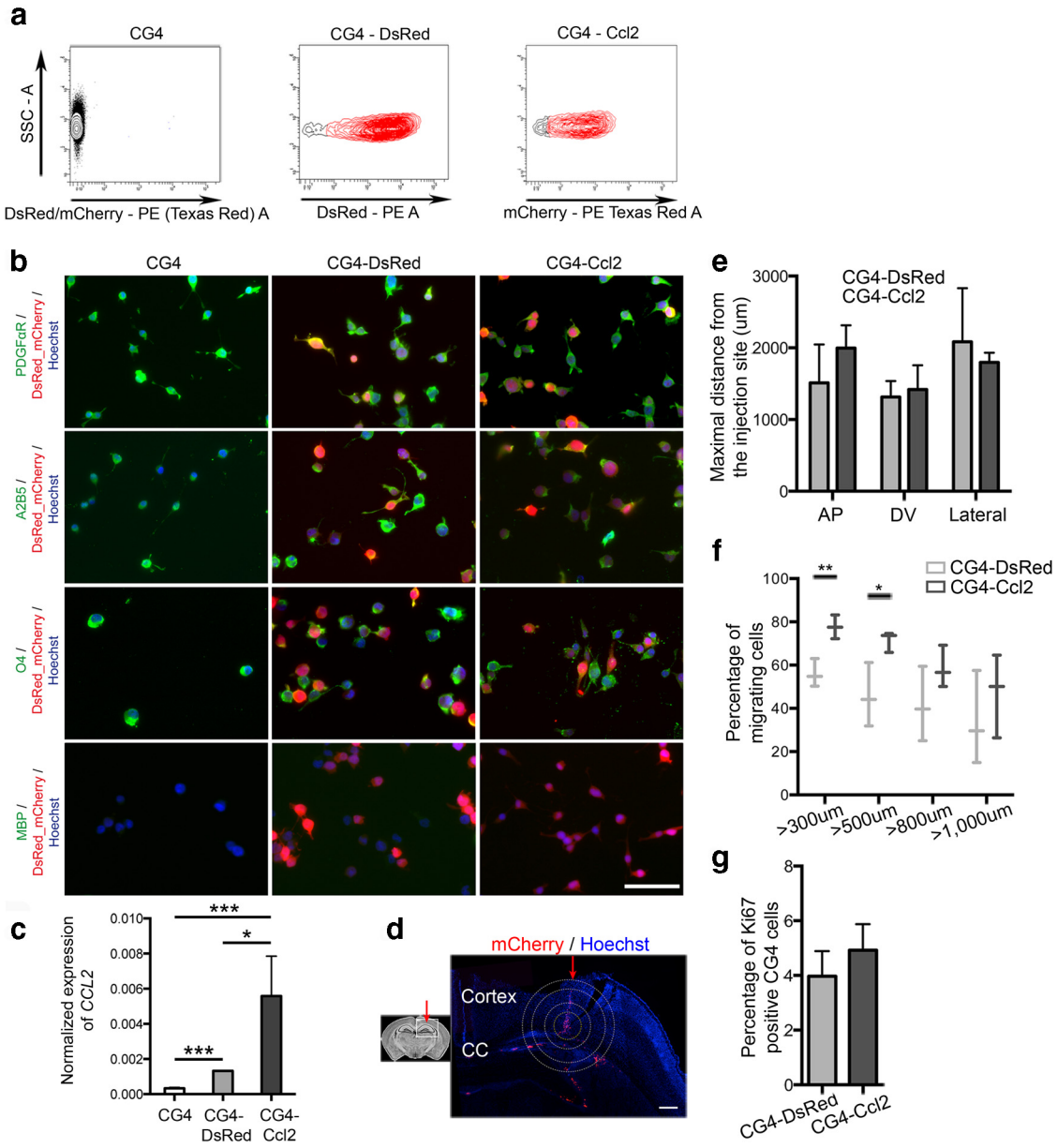

Figure 8. Influence of Ccl2 on aOPC migration *in vivo*. ***a***, Four days after transduction, CG4 transduced with the control (CG4-DsRed) or with the Ccl2 lentivirus (CG4-Ccl2, tagged with mCherry) were sorted. ***b***, CG4 cells were plated and immunostained 4 d after transduction. Scale bar, 50 μm. Nontransduced and transduced CG4 cells express immature markers PDGFαR, A2B5, and O4, but not the mature marker MBP. ***c***, qPCR detection of *CCL2* on nontransduced CG4 cells and transduced CG4 cells (CG4-DSRed or CG4-Ccl2). *CCL2*, expressed at a low level in nontransduced cells, is increased after transduction with the Ccl2 lentivirus ($n = 3$; Student's *t* test, $^{***}p < 0.001$, $^{*}p < 0.05$). Sorted cells are injected in P2 *PDGFαR:GFP* brains. ***d***, The circles represent distances. Scale bar, 200 μm. Red arrow represents the injection track, the inner circle represents the injection site. CC, Corpus callosum. ***e***, No difference in the distance of migration [dorsoventral (DV), anteroposterior (AP), and lateral (Lateral)] was detected between CG4-DsRed and CG4-Ccl2 cells. ***f***, ***g***, Quantification of the percentage of transduced CG4 cells, which have migrated at different distances from the injection site: CG4-Ccl2 cells are more migratory compared to CG4-DsRed cells (***f***), without difference in the percentage of proliferating cells (***g***; $n = 3$; Student's *t* test, $^{**}p < 0.01$, $^{*}p < 0.05$).

negative regulator of OPC differentiation. Analyzing gene expression profiles of the separate stages of spontaneous remyelination in a related model led to the identification of the retinoid acid receptor RXRγ as a major positive regulator of OPC differentiation (Huang et al., 2011).

Using isolated cells maintained in tissue culture, we found that activated aOPCs acquire new capacities for migration and differentiation. We showed that this increased migration corresponds to a chemokinetic effect, with an increased percentage of mobile adult OPCs, without change in the speed of migration. Therefore, aOPCs acquire increased migration and differentiation capacity, both parameters being crucially needed after a demyelinating insult, to reach the demyelinating area and initiate the regenerative process during a window of time when axonal damage is still reversible.

In the cuprizone model, where demyelination and remyelination often occur contemporaneously, it is hazardous to correlate mRNA gene expression changes to a particular stage of the regenerative process. Therefore, to select genes of interest, we took advantage of a gene expression database obtained in a different experimental model, allowing us to distinguish the separate stages of spontaneous remyelination (Huang et al., 2011). In this study, mRNAs were extracted from microdissected lesions that included different cell populations. Our strategy has therefore

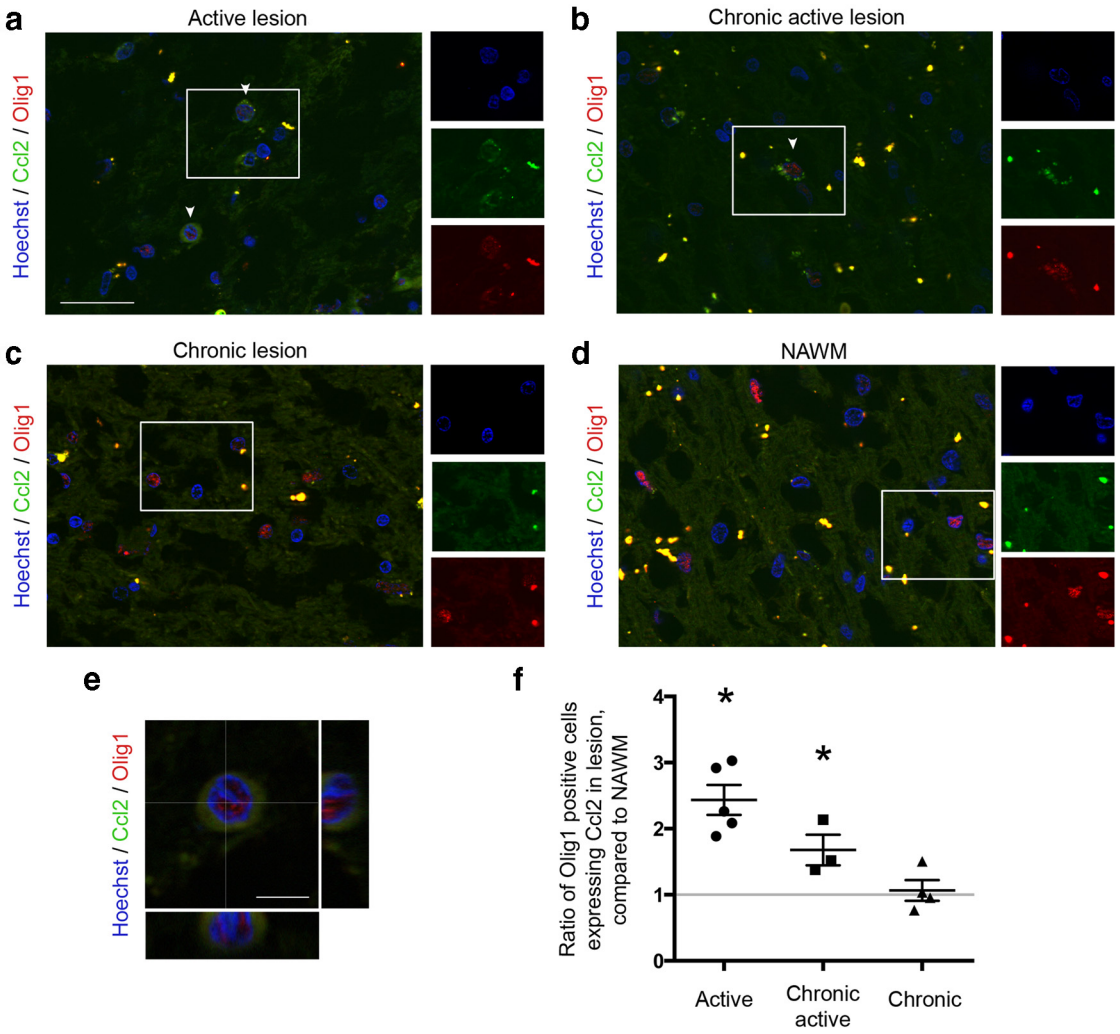

Figure 9. ***a***, ***b***, Ccl2 immunostaining on MS tissues. OPCs (nuclear Olig1 staining) expressing Ccl2 (arrowhead) in an active lesion (***a***) and active borders of a chronic lesion (***b***). ***c***, ***d***, Virtually no Ccl2-expressing OPCs in a chronic lesion (***c***) or NAWM area (***d***). Scale bar, 50 μm. ***e***, High-magnification image of one OPCs, stained by nuclear Olig1 antibody (red), expressing Ccl2 (green). Scale bar, 10 μm. ***f***, Ratio of the percentage of nuclear Olig1-positive cells expressing Ccl2 in multiple sclerosis lesions, compared to adjacent NAWM of the same size ($n = 3–6$, depending on the type of lesion; one-way ANOVA and Holm–Sidak multiple-comparisons test, $^*p < 0.05$).

been to compare our aOPC-specific database and the "early repair database" (14 vs 5 dpl), and to select genes differentially expressed in both databases, which resulted in the identification of 119 genes. These were further analyzed to identify interacting genes, from which emerged two genes of the innate immune system, *IL1β* and *CCL2*. We showed that both Ccl2 and Il1β influenced the motility of aOPCs through Ccr2 and Il1r1 receptors, respectively. In contrast, no effect on differentiation was detected, suggesting that, among the acquired capacities of activated OPCs, increased expression of Ccl2 and Il1β were contributing only to the increased migration. The migratory effect of Ccl2 on aOPCs, which was related neither to receptor expression nor to the stage of differentiation (data not shown), was further confirmed *in vivo*, using gain-of-function experiments.

Both Ccl2 and Il1β are secreted by inflammatory cells and act as chemoattractants (Matsushima et al., 1989; Rollins, 1991). The expression of Ccl2 and Il1β is increased in many different neurological diseases, among them Alzheimer's disease, CNS injury, and MS (Stefini et al., 2008; Sokolova et al., 2009; Hagman et al., 2011). In MS lesions, increased Ccl2 expression has been reported in acute and chronic lesions, and related to the activation and migration of leukocytes and microglial cells (Mahad and Ransohoff, 2003). In addition to inflammatory cells, astrocytes have been shown to express Ccl2 (Glabinski et al., 1996). Using *in vitro* migration assays, several groups have shown that Ccl2 increases the migration of microglia cells, macrophages, monocytes, and neural stem cells (Widera et al., 2004; Opalek et al., 2007; Hinojosa et al., 2011; Iqbal et al., 2013; Li and Tai, 2013). The expression of Il1β or Ccl2 on cells of the oligodendroglial lineage has not been previously reported. Here we show that these cytokines are expressed in aOPCs after experimental demyelination and in MS, and that this expression influences their migration capacity, *in vitro* and *in vivo* (using the CG4 oligodendroglial cell line for the grafting experiments). The migration of nonactivated aOPCs was also enhanced when Ccl2 or Il1β was added to the culture medium. However, *in vitro* migration of activated aOPCs was not affected by the addition of Ccl2 or Il1β, suggesting that activated aOPCs no longer rely on Ccl2 or Il1β (even self-secreted) for an enhanced migration rate. Moreover, in addition to an autocrine effect, the migration of aOPCs might be influenced by the release of Ccl2 or Il1β from neighboring inflammatory cells.

Our results indicate that demyelination-activated OPCs express inflammatory mediators that promote their ability to engage in regeneration by enhancing their ability to respond to

injury by increased motility and ultimately differentiation. Although further experiments with cell-specific loss of function would be needed to decipher this complex interplay between inflammatory cells and regenerative cells, our results hint at a previously unrecognized level of cross talk, which, by changing damaged CNS tissue into an environment conducive to regeneration, offers up new opportunities for enhancing remyelination in clinical situations such as those occurring in MS patients where their powers are waning.

References

Cahoy JD, Emery B, Kaushal A, Foo LC, Zamanian JL, Christopherson KS, Xing Y, Lubischer JL, Krieg PA, Krupenko SA, Thompson WJ, Barres BA (2008) A transcriptome database for astrocytes, neurons, and oligodendrocytes: a new resource for understanding brain development and function. J Neurosci 28:264–278. CrossRef Medline

Emery B, Agalliu D, Cahoy JD, Watkins TA, Dugas JC, Mulinyawe SB, Ibrahim A, Ligon KL, Rowitch DH, Barres BA (2009) Myelin gene regulatory factor is a critical transcriptional regulator required for CNS myelination. Cell 138:172–185. CrossRef Medline

Fancy SP, Zhao C, Franklin RJ (2004) Increased expression of Nkx2.2 and Olig2 identifies reactive oligodendrocyte progenitor cells responding to demyelination in the adult CNS. Mol Cell Neurosci 27:247–254. CrossRef Medline

Fancy SP, Baranzini SE, Zhao C, Yuk DI, Irvine KA, Kaing S, Sanai N, Franklin RJ, Rowitch DH (2009) Dysregulation of the Wnt pathway inhibits timely myelination and remyelination in the mammalian CNS. Genes Dev 23:1571–1585. CrossRef Medline

Fancy SP, Harrington EP, Yuen TJ, Silbereis JC, Zhao C, Baranzini SE, Bruce CC, Otero JJ, Huang EJ, Nusse R, Franklin RJ, Rowitch DH (2011) Axin2 as regulatory and therapeutic target in newborn brain injury and remyelination. Nat Neurosci 14:1009–1016. CrossRef Medline

Ferguson B, Matyszak MK, Esiri MM, Perry VH (1997) Axonal damage in acute multiple sclerosis lesions. Brain 120:393–399. CrossRef Medline

ffrench-Constant C, Raff MC (1986) Proliferating bipotential glial progenitor cells in adult rat optic nerve. Nature 319:499–502. CrossRef Medline

Franklin RJ (2002) Why does remyelination fail in multiple sclerosis? Nat Rev Neurosci 3:705–714. CrossRef Medline

Franklin RJ, Bayley SA, Milner R, ffrench-Constant C, Blakemore WF (1995) Differentiation of the O-2A progenitor cell line CG-4 into oligodendrocytes and astrocytes following transplantation into glia-deficient areas of CNS white matter. Glia 13:39–44. CrossRef Medline

Glabinski AR, Balasingam V, Tani M, Kunkel SL, Strieter RM, Yong VW, Ransohoff RM (1996) Chemokine monocyte chemoattractant protein-1 is expressed by astrocytes after mechanical injury to the brain. J Immunol 156:4363–4368. Medline

Hagman S, Raunio M, Rossi M, Dastidar P, Elovaara I (2011) Disease-associated inflammatory biomarker profiles in blood in different subtypes of multiple sclerosis: prospective clinical and MRI follow-up study. J Neuroimmunol 234:141–147. CrossRef Medline

Hamilton TG, Klinghoffer RA, Corrin PD, Soriano P (2003) Evolutionary divergence of platelet-derived growth factor alpha receptor signaling mechanisms. Mol Cell Biol 23:4013–4025. CrossRef Medline

Hinojosa AE, Garcia-Bueno B, Leza JC, Madrigal JL (2011) CCL2/MCP-1 modulation of microglial activation and proliferation. J Neuroinflammation 8:77. CrossRef Medline

Huang JK, Jarjour AA, Nait Oumesmar B, Kerninon C, Williams A, Krezel W, Kagechika H, Bauer J, Zhao C, Evercooren AB, Chambon P, ffrench-Constant C, Franklin RJ (2011) Retinoid X receptor gamma signaling accelerates CNS remyelination. Nat Neurosci 14:45–53. CrossRef Medline

Iqbal AJ, Regan-Komito D, Christou I, White GE, McNeill E, Kenyon A, Taylor L, Kapellos TS, Fisher EA, Channon KM, Greaves DR (2013) A real time chemotaxis assay unveils unique migratory profiles amongst different primary murine macrophages. PLoS One 8:e58744. CrossRef Medline

Jurevics H, Largent C, Hostettler J, Sammond DW, Matsushima GK, Kleindienst A, Toews AD, Morell P (2002) Alterations in metabolism and gene expression in brain regions during cuprizone-induced demyelination and remyelination. J Neurochem 82:126–136. CrossRef Medline

Klinghoffer RA, Hamilton TG, Hoch R, Soriano P (2002) An allelic series at the PDGFalphaR locus indicates unequal contributions of distinct signaling pathways during development. Dev Cell 2:103–113. CrossRef Medline

Koenning M, Jackson S, Hay CM, Faux C, Kilpatrick TJ, Willingham M, Emery B (2012) Myelin gene regulatory factor is required for maintenance of myelin and mature oligodendrocyte identity in the adult CNS. J Neurosci 32:12528–12542. CrossRef Medline

Koutsoudaki PN, Skripuletz T, Gudi V, Moharregh-Khiabani D, Hildebrandt H, Trebst C, Stangel M (2009) Demyelination of the hippocampus is prominent in the cuprizone model. Neurosci Lett 451:83–88. CrossRef Medline

Le Bras B, Chatzopoulou E, Heydon K, Martínez S, Ikenaka K, Prestoz L, Spassky N, Zalc B, Thomas JL (2005) Oligodendrocyte development in the embryonic brain: the contribution of the plp lineage. Int J Dev Biol 49:209–220. CrossRef Medline

Levine JM, Reynolds R (1999) Activation and proliferation of endogenous oligodendrocyte precursor cells during ethidium bromide-induced demyelination. Exp Neurol 160:333–347. CrossRef Medline

Levine JM, Reynolds R, Fawcett JW (2001) The oligodendrocyte precursor cell in health and disease. Trends Neurosci 24:39–47. CrossRef Medline

Li G, Crang AJ, Rundle JL, Blakemore WF (2002) Oligodendrocyte progenitor cells in the adult rat CNS express myelin oligodendrocyte glycoprotein (MOG). Brain Pathol 12:463–471. Medline

Li X, Tai HH (2013) Activation of thromboxane A2 receptor (TP) increases the expression of monocyte chemoattractant protein-1 (MCP-1)/chemokine (C-C motif) ligand 2 (CCL2) and recruits macrophages to promote invasion of lung cancer cells. PLoS One 8:e54073. CrossRef Medline

Lin G, Mela A, Guilfoyle EM, Goldman JE (2009) Neonatal and adult O4(+) oligodendrocyte lineage cells display different growth factor responses and different gene expression patterns. J Neurosci Res 87:3390–3402. CrossRef Medline

Mahad DJ, Ransohoff RM (2003) The role of MCP-1 (CCL2) and CCR2 in multiple sclerosis and experimental autoimmune encephalomyelitis (EAE). Semin Immunol 15:23–32. CrossRef Medline

Matsushima K, Larsen CG, DuBois GC, Oppenheim JJ (1989) Purification and characterization of a novel monocyte chemotactic and activating factor produced by a human myelomonocytic cell line. J Exp Med 169:1485–1490. CrossRef Medline

Nave KA, Trapp BD (2008) Axon-glial signaling and the glial support of axon function. Annu Rev Neurosci 31:535–561. CrossRef Medline

Opalek JM, Ali NA, Lobb JM, Hunter MG, Marsh CB (2007) Alveolar macrophages lack CCR2 expression and do not migrate to CCL2. J Inflamm (Lond) 4:19. CrossRef Medline

Piaton G, Aigrot MS, Williams A, Moyon S, Tepavcevic V, Moutkine I, Gras J, Matho KS, Schmitt A, Soellner H, Huber AB, Ravassard P, Lubetzki C (2011) Class 3 semaphorins influence oligodendrocyte precursor recruitment and remyelination in adult central nervous system. Brain 134:1156–1167. CrossRef Medline

Robinson S, Miller RH (1999) Contact with central nervous system myelin inhibits oligodendrocyte progenitor maturation. Dev Biol 216:359–368. CrossRef Medline

Rollins BJ (1991) JE/MCP-1: an early-response gene encodes a monocyte-specific cytokine. Cancer Cells 3:517–524. Medline

Ruffini F, Arbour N, Blain M, Olivier A, Antel JP (2004) Distinctive properties of human adult brain-derived myelin progenitor cells. Am J Pathol 165:2167–2175. CrossRef Medline

Shen S, Sandoval J, Swiss VA, Li J, Dupree J, Franklin RJ, Casaccia-Bonnefil P (2008) Age-dependent epigenetic control of differentiation inhibitors is critical for remyelination efficiency. Nat Neurosci 11:1024–1034. CrossRef Medline

Shields SA, Gilson JM, Blakemore WF, Franklin RJ (1999) Remyelination occurs as extensively but more slowly in old rats compared to young rats following gliotoxin-induced CNS demyelination. Glia 28:77–83. CrossRef Medline

Silvestroff L, Bartucci S, Pasquini J, Franco P (2012) Cuprizone-induced demyelination in the rat cerebral cortex and thyroid hormone effects on cortical remyelination. Exp Neurol 235:357–367. CrossRef Medline

Skripuletz T, Lindner M, Kotsiari A, Garde N, Fokuhl J, Linsmeier F, Trebst C, Stangel M (2008) Cortical demyelination is prominent in the murine cuprizone model and is strain-dependent. Am J Pathol 172:1053–1061. CrossRef Medline

Sokolova A, Hill MD, Rahimi F, Warden LA, Halliday GM, Shepherd CE (2009) Monocyte chemoattractant protein-1 plays a dominant role in the chronic inflammation observed in Alzheimer's disease. Brain Pathol 19: 392–398. CrossRef Medline

Spassky N, Olivier C, Cobos I, LeBras B, Goujet-Zalc C, Martínez S, Zalc B, Thomas JL (2001) The early steps of oligodendrogenesis: insights from the study of the plp lineage in the brain of chicks and rodents. Dev Neurosci 23:318–326. CrossRef Medline

Spassky N, de Castro F, Le Bras B, Heydon K, Quéraud-LeSaux F, Bloch-Gallego E, Chédotal A, Zalc B, Thomas JL (2002) Directional guidance of oligodendroglial migration by class 3 semaphorins and netrin-1. J Neurosci 22:5992–6004. Medline

Stefini R, Catenacci E, Piva S, Sozzani S, Valerio A, Bergomi R, Cenzato M, Mortini P, Latronico N (2008) Chemokine detection in the cerebral tissue of patients with posttraumatic brain contusions. J Neurosurg 108: 958–962. CrossRef Medline

Syed YA, Baer AS, Lubec G, Hoeger H, Widhalm G, Kotter MR (2008) Inhibition of oligodendrocyte precursor cell differentiation by myelin-associated proteins. Neurosurg Focus 24:E5. CrossRef Medline

Widera D, Holtkamp W, Entschladen F, Niggemann B, Zänker K, Kaltschmidt B, Kaltschmidt C (2004) MCP-1 induces migration of adult neural stem cells. Eur J Cell Biol 83:381–387. CrossRef Medline

Zawadzka M, Rivers LE, Fancy SP, Zhao C, Tripathi R, Jamen F, Young K, Goncharevich A, Pohl H, Rizzi M, Rowitch DH, Kessaris N, Suter U, Richardson WD, Franklin RJ (2010) CNS-resident glial progenitor/stem cells produce Schwann cells as well as oligodendrocytes during repair of CNS demyelination. Cell Stem Cell 6:578–590. CrossRef Medline